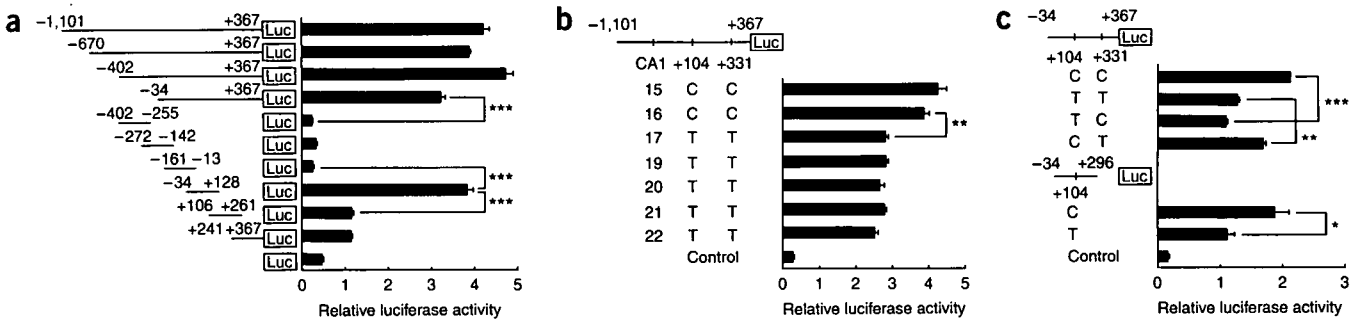

Figure 2 Analysis of *GDF5* promoter activity in HCS-2/8 cells. Horizontal bars indicate deletion constructs, and horizontal columns indicate relative luciferase activities. Nucleotide positions (start and end) are shown above bars, and sequence variations are indicated below bars. (**a**) Localization of *GDF5* promoter activity. The most significant SNP (+104T/C) is contained within the core promoter. (**b**) Allelic differences in luciferase activity among seven haplotypes containing one dinucleotide-repeat polymorphism (CA1; 4192660–4192703 of NT_028392 in **Supplementary Table 3**) and two SNPs (+104T/C and +331T/C). Observed allelic differences depend on the SNPs. (**c**) Localization of allelic differences in the *GDF5* promoter. The osteoarthritis susceptibility allele (+104T) accounts for the lower luciferase activities. Data represent mean ± s.e.m. in triplicate assays. $^*P < 0.05$, $^{**}P < 0.01$, $^{***}P < 0.001$ (Student's *t*-test).

amplified 5 ng of genomic DNA with fluorescence-labeled primers (Applied Biosystems); products were examined using an ABI 3700 DNA analyzer (Applied Biosystems).

5′- and 3′-RACE. We performed 5′ and 3′ RACE using human fetus, bone marrow and fetal brain Marathon-Ready cDNAs (Clontech), along with cDNA libraries constructed from three chondrogenic cell lines (OUMS-27 (ref. 27), HCS-2/8 (ref. 28) and CS-OKB (ref. 29)) using the FastTrack 2.0 mRNA Isolation kit (Invitrogen) and Smart cDNA Library Construction Kit (Clontech). Amplified fragments from each source gave a single band on agarose gel electrophoresis and were cloned into the pCR-XL-TOPO vector (Invitrogen).

Luciferase assay. Genomic fragments were amplified using KOD-Plus polymerase (TOYOBO) using primers that introduced restriction sites at the 5′ end for the promoter assay (*Kpn*I or *Hin*dIII) or the enhancer assay (*Bam*HI or *Sal*I). Amplified fragments were cloned into the pCR-Blunt II-TOPO vector (Invitrogen). After sequence verification, fragments were subcloned into the pGL3-basic vector (Promega). HCS-2/8 cells were cultured in DMEM supplemented with 10% FBS. For each transfection, 5×10^4 cells were transfected with 0.8 μg of experimental vector and 4 ng of pRL-TK as an internal control, using FuGene 6 Transfection Reagent (Roche). After 48 h, cells were harvested and luciferase activity was measured using the PicaGene Dual Sea Pansy system (Toyo Ink).

Statistical and haplotype analyses. We evaluated genotypic, allelic, dominant and recessive models in the case-control study using the χ^2-test or Fisher's exact test. Haplotype frequencies were estimated with the EM algorithm[30], using the Web-based programs SNPHAP (http://www-gene.cimr.cam.ac.uk/clayton/software/) and EH (http://www.genemapping.cn/eh.htm). The linkage disequilibrium indices D' and Δ (ref. 30) and the χ^2-test for Hardy-Weinberg equilibrium were calculated using spreadsheet software (Excel).

Accession numbers. GenBank mRNA sequence for growth differentiation factor 5 (*GDF5*), NM_000557.

Note: Supplementary information is available on the Nature Genetics website.

ACKNOWLEDGMENTS

We thank individuals for participating the study. We also thank K. Toyoshima, A. Kotani, K. Nakamura, A. Fukuda, A. Kawakami, H. Mototani and E. Nakashima for help in collecting samples and performing the experimental study and Y. Takanashi and T. Kusadokoro for technical assistance.

AUTHOR CONTRIBUTIONS

Y.M. performed the Japanese knee osteoarthritis association study and prepared the manuscript. A.M. performed the hip association study, *in vitro* functional assay and prepared the manuscript. D.S. performed the Chinese association study. T.K., Y.T., S.S., M.F., A.S., A.U., S.Y., K.O. and Y.N. managed DNA sample and clinical information, and contributed data interpretation. K.O. and M.T. contributed to cell experiments. T.T. contributed to data analysis and manuscript preparation. Q.J. managed the Chinese association study. S.I. planned and supervised the whole project.

COMPETING INTERESTS STATEMENT

The authors declare no competing financial interests.

Published online at http://www.nature.com/naturegenetics
Reprints and permissions information is available online at http://npg.nature.com/reprintsandpermissions

1. Kellgren, J.H. & Moore, R. Generalized osteoarthritis and Heberden's nodes. *Br. Med. J.* **1**, 181–187 (1952).
2. Oliveria, S.A., Felson, D.T., Reed, J.I., Cirillo, P.A. & Walker, A.M. Incidence of symptomatic hand, hip, and knee osteoarthritis among patients in a health maintenance organization. *Arthritis Rheum.* **38**, 1134–1141 (1995).
3. Felson, D.T. & Zhang, Y. An update on the epidemiology of knee and hip osteoarthritis with a view to prevention. *Arthritis Rheum.* **41**, 1343–1355 (1998).
4. Stecher, R.M. Heberden's nodes: heredity in hypertrophic arthritis of the finger joints. *Am. J. Med. Sci.* **201**, 801–809 (1941).
5. Kellgren, J.H., Lawrence, J.S. & Bier, F. Genetic factors in generalized osteo-arthrosis. *Ann. Rheum. Dis.* **22**, 237–255 (1963).
6. Francis-West, P.H. *et al.* Mechanisms of GDF-5 action during skeletal development. *Development* **126**, 1305–1315 (1999).
7. Merino, R. *et al.* Expression and function of Gdf-5 during digit skeletogenesis in the embryonic chick leg bud. *Dev. Biol.* **206**, 33–45 (1999).
8. Storm, E.E. *et al.* Limb alterations in brachypodism mice due to mutations in a new member of the TGFβ-superfamily. *Nature* **368**, 639–643 (1994).
9. Thomas, J.T. *et al.* A human chondrodysplasia due to a mutation in a TGF-β superfamily member. *Nat. Genet.* **12**, 315–317 (1996).
10. Erlacher, L. *et al.* Cartilage-derived morphogenetic proteins and osteogenic protein-1 differentially regulate osteogenesis. *J. Bone Miner. Res.* **13**, 383–392 (1998).
11. Wolfman, N.M. *et al.* Ectopic induction of tendon and ligament in rats by growth and differentiation factors 5, 6, and 7, members of the TGF-β gene family. *J. Clin. Invest.* **100**, 321–330 (1997).
12. Tsumaki, N. *et al.* Role of CDMP-1 in skeletal morphogenesis: promotion of mesenchymal cell recruitment and chondrocyte differentiation. *J. Cell Biol.* **144**, 161–173 (1999).
13. Faiyaz-Ul-Haque, M. *et al.* Frameshift mutation in the cartilage-derived morphogenetic protein 1 (CDMP1) gene and severe acromesomelic chondrodysplasia resembling Grebe-type chondrodysplasia. *Am. J. Med. Genet.* **111**, 31–37 (2002).
14. Savarirayan, R. *et al.* Broad phenotypic spectrum caused by an identical heterozygous CDMP-1 mutation in three unrelated families. *Am. J. Med. Genet. A* **117**, 136–142 (2003).
15. Sugiura, T., Hotten, G. & Kawai, S. Minimal promoter components of the human growth/differentiation factor-5 gene. *Biochem. Biophys. Res. Commun.* **263**, 707–713 (1999).
16. Freedman, M.L. *et al.* Assessing the impact of population stratification on genetic association studies. *Nat. Genet.* **36**, 388–393 (2004).
17. Chang, S.C. *et al.* Cartilage-derived morphogenetic proteins. New members of the transforming growth factor-beta superfamily predominantly expressed in long bones during human embryonic development. *J. Biol. Chem.* **269**, 28227–28234 (1994).

18. Storm, E.E. & Kingsley, D.M. GDF5 coordinates bone and joint formation during digit development. *Dev. Biol.* **209**, 11–27 (1999).
19. Hotten, G.C. *et al.* Recombinant human growth/differentiation factor 5 stimulates mesenchyme aggregation and chondrogenesis responsible for the skeletal development of limbs. *Growth Factors* **13**, 65–74 (1996).
20. Bobacz, K. *et al.* Cartilage-derived morphogenetic protein-1 and -2 are endogenously expressed in healthy and osteoarthritic human articular chondrocytes and stimulate matrix synthesis. *Osteoarthritis Cartilage* **10**, 394–401 (2002).
21. Kizawa, H. *et al.* An aspartic acid repeat polymorphism in asporin inhibits chondrogenesis and increases susceptibility to osteoarthritis. *Nat. Genet.* **37**, 138–144 (2005).
22. Mabuchi, A. *et al.* Identification of sequence polymorphisms of the COMP (cartilage oligomeric matrix protein) gene and association study in osteoarthrosis of the knee and hip joints. *J. Hum. Genet.* **46**, 456–462 (2001).
23. Mototani, H. *et al.* A functional single nucleotide polymorphism in the core promoter region of CALM1 is associated with hip osteoarthritis in Japanese. *Hum. Mol. Genet.* **14**, 1009–1017 (2005).
24. Ikeda, T. *et al.* Identification of sequence polymorphisms in two sulfation-related genes, PAPSS2 and SLC26A2, and an association analysis with knee osteoarthritis. *J. Hum. Genet.* **46**, 538–543 (2001).
25. Jiang, Q. *et al.* Replication of the association of the aspartic acid repeat polymorphism in the asporin gene with knee-osteoarthritis susceptibility in Han Chinese. *J. Hum. Genet.* **51**, 1068–1072 (2006).
26. Ohnishi, Y. *et al.* A high-throughput SNP typing system for genome-wide association studies. *J. Hum. Genet.* **46**, 471–477 (2001).
27. Kunisada, T. *et al.* A new human chondrosarcoma cell line (OUMS-27) that maintains chondrocytic differentiation. *Int. J. Cancer* **77**, 854–859 (1998).
28. Takigawa, M. *et al.* Establishment of a clonal human chondrosarcoma cell line with cartilage phenotypes. *Cancer Res.* **49**, 3996–4002 (1989).
29. Chano, T. *et al.* Characterization of a newly established human chondrosarcoma cell line, CS-OKB. *Virchows Arch.* **432**, 529–534 (1998).
30. Ott, J. Counting methods (EM algorithm) in human pedigree analysis: linkage and segregation analysis. *Ann. Hum. Genet.* **40**, 443–454 (1977).

J Hum Genet (2007) 52:220–229
DOI 10.1007/s10038-006-0102-5

ORIGINAL ARTICLE

A functional SNP in *ITIH3* is associated with susceptibility to myocardial infarction

Yusuke Ebana · Kouichi Ozaki · Katsumi Inoue · Hiroshi Sato · Aritoshi Iida · Htay Lwin · Susumu Saito · Hiroya Mizuno · Atsushi Takahashi · Takahiro Nakamura · Yoshinari Miyamoto · Shiro Ikegawa · Keita Odashiro · Masakiyo Nobuyoshi · Naoyuki Kamatani · Masatsugu Hori · Mitsuaki Isobe · Yusuke Nakamura · Toshihiro Tanaka

Received: 3 November 2006 / Accepted: 1 December 2006 / Published online: 9 January 2007

Abstract Myocardial infarction (MI) results from complex interactions of multiple genetic and environmental factors. To disclose genetic backgrounds of MI, we performed a large-scale, case-control association study using 52,608 gene-based single-nucleotide polymorphism (SNP) markers, and identified a candidate SNP located on chromosome 3p21.2–p21.1. Subsequent linkage–disequilibrium mapping indicated very significant association between MI and a SNP in exon 2 of the inter-alpha (globulin) inhibitor 3 gene (*ITIH3*; $\chi^2 = 24.88$, $P = 6.1 \times 10^{-7}$, 3,353 affected individuals versus 3,807 controls). In vitro functional analyses showed that this SNP enhanced the transcriptional level of the ITIH3 gene. Furthermore, we found expression of the ITIH3 protein in the vascular smooth muscle cells and macrophages in the human atherosclerotic lesions, suggesting *ITIH3* SNP to be a novel genetic risk factor of MI.

Keywords Functional analysis · Linkage–disequilibrium mapping · Myocardial infarction · Single-nucleotide polymorphism markers

Y. Ebana · K. Ozaki · H. Lwin · T. Tanaka (✉)
Laboratory for Cardiovascular Diseases, SNP Research Center, The Institute of Physical and Chemical Research (RIKEN), 4-6-1 Shirokanedai, Minato-ku, Tokyo 108-8639, Japan
e-mail: toshitan@ims.u-tokyo.ac.jp

Y. Ebana · M. Isobe
Department of Cardiovascular Medicine, Tokyo Medical and Dental University, Tokyo, Japan

K. Inoue · K. Odashiro · M. Nobuyoshi
Department of Cardiology, Kokura Memorial Hospital, Kitakyushu 802-8555, Japan

H. Sato · H. Mizuno · M. Hori
Department of Internal Medicine and Therapeutics, Osaka University Graduate School of Medicine, Suita, Japan

A. Iida · S. Saito · Y. Nakamura
Laboratory for Pharmacogenetics, SNP Research Center, The Institute of Physical and Chemical Research (RIKEN), Tokyo, Japan

A. Takahashi · T. Nakamura · N. Kamatani
Laboratory for Statistical Analysis, SNP Research Center, The Institute of Physical and Chemical Research (RIKEN), Tokyo, Japan

Y. Miyamoto · S. Ikegawa
Laboratory for Bone and Joint Disease, SNP Research Center, The Institute of Physical and Chemical Research (RIKEN), Tokyo, Japan

Introduction

Coronary artery diseases, including myocardial infarction (MI), have been one of major leading causes of death in the developed countries (Ross 1999). Multiple lines of evidence have revealed several coronary risk factors contributing to the development of atherosclerosis (Libby 2002). Although each factor by itself seems partly under genetic control, a positive family history is an independent predictor (Shea et al. 1984), which implies genetic contribution to MI. Numerous reports based on family and/or twin studies have provided evidence for a genetic component in the etiology of MI (Marenberg et al. 1996). In recent years, candidate MI susceptibility genes were identified on several chromosome loci using linkage analysis (Wang et al. 2004) and/or single-nucleotide polymorphism (SNP)

case-control association studies (Yamada et al. 2002; Ozaki et al. 2002, 2004, 2006; Helgadottir et al. 2004).

Inflammation is thought to contribute to atherosclerosis and increase the risk of MI (Libby 2002). It is a consequence of complex interactions among modified lipoproteins, monocyte-derived macrophages, T lymphocytes, and vascular smooth muscle cells (SMCs) from the vessel wall. Recent studies have shown the importance of chemoattractants, e.g., adhesion molecules (Cybulsky and Gimbrone 1991), chemokines (Boring et al. 1998), growth factors (Brogi et al. 1993), and proteolytic enzymes and their inhibitors (Galis et al. 1994), in atherosclerotic plaque formation and rupture.

Inter-alpha (globulin) inhibitor 3 (ITIH3), one of the constituents of plasma serine protease inhibitors, has been shown to be related to the proinflammatory process (Fries and Kaczmarczyk 2003). ITIH3 protein is characterized by its unique covalent binding to the chondroitin sulfate chain of bikunin proteoglycan (Zhuo et al. 2004). This complex, named pre-alpha trypsin inhibitor (PαI) is synthesized by hepatocytes and released to the blood vessel upon stimulation of the proinflammatory cytokines (tumor necrosis factor or interleukin-1). Then, ITIH3 makes a complex with the locally synthesized hyaluronan (HA) and interacts with inflammatory cells (Fries and Kaczmarczyk 2003). ITIH3-HA complex has been reported to be involved in inflammatory diseases, including rheumatoid arthritis and inflammatory bowel diseases (Zhuo et al. 2004).

We report here identification of a significant association of a SNP in *ITIH3* with MI through a large-scale association study using approximately 50,000 gene-based SNPs. We also analyzed its functional significance indicating a possible role of this genetic variation in the pathogenesis of MI.

Materials and methods

DNA samples

The study included Japanese individuals with MI who were referred to the Osaka Acute Coronary Insufficiency Study group. The diagnosis of definite MI has been described previously (Ohnishi et al. 2000; Ozaki et al. 2002). The control subjects consisted of general populations recruited through several medical institutes in Japan. Clinical characteristics have been described previously (Ozaki et al. 2006). All subjects were Japanese and provided written informed consent to participation in the study or, if they were under 20 years old, their parents gave consent according to the process approved by the Ethical Committee at the SNP Research Center, The Institute of Physical and Chemical Research (RIKEN), Yokohama.

Table 1 Distribution of *P* values in the first stage screening of 188 cases and 752 controls

P value	Number of SNPs	
	Recessive association	Dominant association
>0.01	48,669	48,818
<0.01	442	322
<0.001	48	23
<0.0001	5	4
<0.00001	3	0

Genotyping

Designs for polymerase chain reaction (PCR) primers, PCR experiments, DNA extraction, DNA sequencing, SNP discovery, genotyping of SNPs and statistical analysis have been described previously (Ohnishi et al. 2001; Ozaki et al. 2002).

Haplotype block

We used Haploview software for the identification of haplotype. We adopted the solid spine of LD for analysis and extended spine if $D' > 0.90$. We defined strong LD if the one-sided upper 95% confidence boundary on D' was >0.98 and the lower boundary was <0.80. Conversely, we defined strong recombination pairs for which the upper confidence bound on D' was less than 0.90.

Luciferase assay

DNA fragments corresponding to nt 642 of intron 1 to 54 of intron 2 of *ITIH3* were amplified by PCR using genomic DNA as template, and cloned into pGL3-promotor vector (Promega) in the 5′–3′ orientation. For the SV40-SNP-luciferase construct for *ITIH3* SNP and all constructs for *ITIH1* SNP, double-stranded oligonucleotides (nt 695 of intron 1 to 21 of intron 2 for *ITIH3* and nt 517 to 551 of intron 10 for *ITIH1*) were cloned into pGL3-promoter vector. We grew Jurkat cells and HepG2 cells (obtained from RIKEN Cell Bank; RCB0806, RCB1681, respectively) in RPMI1640 medium and Dulbecco's modified eagle medium (DMEM), respectively, supplemented with 10% fetal bovine serum. We then transfected cells (approximately 1×10^5 and 3×10^6 cells in HepG2 and Jurkat cells, respectively) with 1 μg of either construct and

Table 2 Association analysis of SNPs in the third stage screening

Genotype	MI (%)	CO (%)	Statistical test	Allele frequency	Dominant model
rs2286797					
GG	2,022 (60.3)	2,094 (55.0)	χ^2	24.88	20.49
GA	1,161 (34.6)	1,449 (38.1)	*P* value	6.1×10^{-7}	6.0×10^{-6}
AA	170 (5.1)	264 (6.9)	Odds ratio	1.216	1.243
Total	3,353 (100)	3,807 (100)	95% CI	1.126–1.313	1.131–1.365
rs2301523[a]					
GG	2,919 (84.3)	3,364 (88.1)	χ^2	22.71	22.37
GA	528 (15.2)	445 (11.7)	*P* value	1.9×10^{-6}	2.3×10^{-6}
AA	17 (0.5)	10 (0.3)	Odds ratio	1.362	1.38
Total	3,464 (100)	3,819 (100)	95% CI	1.199–1.547	1.207–1.578
rs2074396					
CC	1,354 (40.3)	1,523 (40.5)	χ^2	0.00	0.00
CA	1,557 (46.4)	1,740 (46.2)	*P* value	0.95	0.98
AA	446 (13.3)	501 (13.3)	Odds ratio	1.002	1.002
Total	3,357 (100)	3,764 (100)	95% CI	0.936–1.073	0.874–1.149
rs989437					
AA	2,122 (65.8)	2,396 (64.0)	χ^2	1.96	0.07
GA	971 (30.1)	1,188 (31.7)	*P* value	0.16	0.79
GG	133 (4.1)	159 (4.2)	Odds ratio	1.062	1.032
Total	3,226 (100)	3,743 (100)	95% CI	0.976–1.155	0.976–1.155
rs2240999					
GG	2,544 (75.4)	2,947 (78.0)	χ^2	8.06	4.23
GC	767 (22.7)	786 (20.8)	*P* value	0.0045	0.04
CC	61 (1.8)	46 (1.2)	Odds ratio	1.155	1.495
Total	3,372 (100)	3,779 (100)	95% CI	1.046–1.276	1.017–2.199
rs2242421					
GG	1,400 (41.6)	1,485 (41.6)	χ^2	0.57	0.42
GA	1,502 (44.6)	1,748 (46.9)	*P* value	0.45	0.52
AA	462 (13.7)	492 (13.2)	Odds ratio	1.027	1.046
Total	3,364 (100)	3,725 (100)	95% CI	0.959–1.100	0.913–1.199
rs2242442					
GG	1,072 (32.0)	1,143 (30.6)	χ^2	0.26	0.4
GA	1,605 (47.9)	1,868 (50.0)	*P* value	0.61	0.53
AA	672 (20.1)	728 (19.5)	Odds ratio	1.017	1.038
Total	3,349 (100)	3,739 (100)	95% CI	0.952–1.087	0.924–1.167
rs2292428					
TT	1,631 (48.4)	1,844 (49.1)	χ^2	0.51	0.39
TC	1,425 (42.3)	1,580 (42.1)	*P* value	0.48	0.53
CC	313 (9.3)	333 (8.9)	Odds ratio	1.026	1.053
Total	3,369 (100)	3,767 (100)	95% CI	0.955–1.103	0.896–1.238
rs2290140					
CC	1,810 (54.9)	2,099 (56.7)	χ^2	2.96	1.23
CT	1,265 (38.3)	1,373 (37.1)	*P* value	0.085	0.27
TT	224 (6.8)	227 (6.1)	Odds ratio	1.069	1.114
Total	3,299 (100)	3,699 (100)	95% CI	0.991–1.154	0.921–1.348
rs3748037					
CC	1,604 (47.5)	1,796 (47.8)	χ^2	0.28	0.65
CT	1,435 (42.5)	1,610 (42.8)	*P* value	0.6	0.42
TT	336 (10.0)	353 (9.4)	Odds ratio	1.019	1.067
Total	3,375 (100)	3,759 (100)	95% CI	0.949–1.094	0.912–1.248
rs1043228					
CC	3,205 (95.2)	3,623 (96.0)	χ^2	2.92	0.02
CT	159 (4.7)	147 (3.9)	*P* value	0.087	0.89
TT	3 (0.1)	3 (0.1)	Odds ratio	1.214	1.121
Total	3,367 (100)	3,773 (100)	95% CI	0.972–1.516	0.226–5.556
rs220079					
TT	1,046 (30.9)	1,240 (32.9)	χ^2	2.04	0.21
TC	1,703 (50.4)	1,841 (48.8)	*P* value	0.15	0.65
CC	632 (18.7)	689 (18.3)	Odds ratio	1.049	1.028
Total	3,381 (100)	3,770 (100)	95% CI	0.982–1.121	0.912–1.159
rs2808707					
GG	921 (27.3)	1,058 (28.3)	χ^2	1.99	2.04

Table 2 Continued

Genotype	MI (%)	CO (%)	Statistical test	Allele frequency	Dominant model
GT	1,660 (49.3)	1,861 (49.7)	*P* value	0.16	0.15
TT	789 (23.4)	823 (22.0)	Odds ratio	1.049	1.084
Total	3,370 (100)	3,742 (100)	95% CI	0.982–1.120	0.970–1.212
rs3793136					
TT	3,113 (92.5)	3,510 (92.7)	χ^2	0.18	0.93
TC	249 (7.4)	275 (7.3)	*P* value	0.67	0.34
CC	4 (0.1)	2 (0.1)	Odds ratio	1.038	2.252
Total	3,366 (100)	3,790 (100)	95% CI	0.873–1.233	0.412–12.301

[a] Reported by Ishii et al. (21)

Table 3 Power of screening strategy

	First	Second	Third	Total
Additive model	0.25	0.45	0.90	0.10
Dominant model	0.39	0.76	0.99	0.29
Recessive model	0.41	0.57	0.97	0.23

0.1 μg of pRL-TK vector, an internal control for transfection efficiency, using FuGene transfection reagent (Roche). After 24 h, we collected cells and measured luciferase activity using the Dual-Luciferase Reporter Assay System (Promega; Ozaki et al. 2002).

Electrophoretic mobility-shift assay

We prepared nuclear extracts from Jurkat cells, HCASMCs and HCAECs (Cambrex) as previously described, and then incubated them with three tandem copies of 16 oligonucleotides (8 of exon 2 to 2 of intron 3 of *ITIH3*) labeled with digoxigenen –11-ddUTP using the digoxigenin gel-shift kit (Roche). For competition studies, we pre-incubated nuclear extract with unlabeled oligonucleotide (100-fold excess) before adding digoxigenin-labeled oligonucleotide. We separated the protein-DNA complexes on a non-denaturing 7% polyacrylamide gel in 0.5 × Tris–Borate–EDTA buffer. We transferred the gel to nitrocellulose membrane and detected the signal with a chemiluminescent detection system (Roche) according to the manufacturer's instructions (Ozaki et al. 2002).

Immunohistochemistry

Tissue samples were obtained from patients with MI by elective directional coronary atherectory after obtaining informed consent. Immunohistochemical protocols were carried out as described previously using goat polyclonal anti-human ITIH3 IgG (Santa Cruz) (Minami et al. 2001; Ozaki et al. 2004).

Statistical analysis

We carried out statistical analyses for the association study, haplotype frequencies and Hardy–Weinberg equilibrium and calculation of r^2 as described elsewhere (Yamada et al. 2001). We calculated the total number of independent SNPs in this study to be 41,362 (the SNPs in LD, $r^2 > 0.80$, were considered as one SNP) and used this to correct the obtained *P* value by the Bonferroni's correction (P_c). The result of luciferase assay were tested using Fisher's exact test (Statistica software, StatSoft), and mRNA stability data were tested using Student *t* test.

Results

Association study

We first genotyped randomly-selected 188 MI patients and 752 general Japanese population, using a high-throughput multiplex PCR-Invader assay method (Ohnishi et al. 2001) using 52,608 gene-based tag SNPs selected from the JSNP database (Haga et al. 2002; Tsunoda et al. 2004). We successfully obtained the genotype information at 49,167 SNP loci and the distribution of *P* values for these SNPs is summarized in Table 1. We further genotyped SNPs that showed *P* value of 0.01 or smaller with a larger panel of individuals (664 MI and 1,473 controls) as the second-stage screening. Through this screening, we found 14 loci revealing *P* values of 0.001 or smaller, and further verified their associations with MI by genotyping 3,353 affected and 3,807 control individuals. Of two SNPs that we considered to have the statistically-significant association (Table 2), one SNP was located within *MIAT* (Ishii et al. 2006) and the other was present in exon 2 (rs2286797) of the *ITIH3* gene on chromosome 3p21.2–p21.1 ($P = 6.1 \times 10^{-7}$; comparison of allele

Table 4 Identified polymorphisms in *ITIH1* and *ITIH3*

Polymorphism position[a]	rs number	MAF[b]
ITIH1		
Intron 2 188G > A	–	0.021
Intron 5 646A > T	rs2302417	0.490
Intron 6 1327G > A	–	0.021
Intron 6 1507T > C	rs2710323	0.500
Intron 8 304–305 GTGCCGGGAGTAA/ins	rs3836493	0.486
Exon 10 1197C > G, I399M	rs12638839	0.021
Intron 10 238C > T	rs2710322	0.259
Intron 10 320G > A	rs3774354	0.472
Intron 10 423G > A	rs3774355	0.471
Intron 10 536A > C	rs3774356	0.261
Intron 11 87G > A	rs2239551	0.492
Intron 12 82T > A	rs2268023	0.492
Exon 14 1754A > T, E585V	rs678	0.489
Exon 14 1784A > G, E595R	rs1042779	0.492
Intron 14 36A > G	rs2286799	0.041
Intron 14 62A > C	rs2286798	0.487
Intron 15 148C > G	–	0.023
Intron 15 299G > C	–	0.022
Intron 18 428T > C	rs2284351	0.492
Intron 18 1069T > G	rs4687550	0.483
Intron 18 1087T > C	rs4687551	0.483
Exon 19 2196G > A, R732R	–	0.041
Exon 19 2311C > T, R771W	–	0.041
Intron 19 224A > C	rs2270197	0.492
Intron 20 347–348 G/ins	rs3216516	0.483
Intron 20 525T > C	rs1076425	0.492
Intron 20 591T > C	rs1075653	0.500
Exon 21 2547T > C, S849S	rs9324	0.497
Intron 21 121T > C	–	0.005
ITIH3		
Promoter –1254G > A	rs4687654	0.489
Promoter –905C > T	rs2239699	0.487
Promoter –217C > T	–	0.063
Promoter –192C > T	rs9881468	0.457
Exon 2 108G > A, P36P	rs2286797	0.249
Exon 4 291C > T, D291D	rs2240921	0.001
Intron 4 150C > T	rs2240920	0.481
Intron 4 418C > G	rs2240919	0.482
Intron 7 112G > A	rs2535629	0.474
Exon 9 943C > A, K943Q	rs3617	0.495
Intron 11 24C > T	–	0.027
Intron 11 192C > T	rs736408	0.456
Intron 13 851T > C	rs4481150	0.478
Intron 13 1033T > C	rs2710331	0.459
Intron 14 377T > C	rs4687552	0.458
Intron 19 39G > C	rs2276813	0.006
Intron 19 99G > A	rs13059141	0.024
Intron 21 327C > T	rs3815421	0.004

– The variant was not included in the dbSNP database (build 126)

[a] Nucleotide numbering is according to the mutation nomenclature (den Dunnen and Antonarakis 2000)

[b] Minor allele frequency

frequency, Table 2). Even after Bonferroni's correction, this result was considered to be statistically significant ($P_c < 0.05$). Through the calculation by FDR (Storey 2002) and the association was unlikely to be false positive (q value = 8.86×10^{-4}). Detection power of this strategy for association under the condition of odds ratio of 1.5 and MAF of 0.40 is shown in Table 3.

Since another SNP(s) in this locus might confer a genetic risk of MI, we searched the HapMap database (http://www.hapmap.org; The international HapMap Consortium 2003) and found that *ITIH3* as well as *ITIH1*, both of which belong to the ITIH family, were contained in the same haplotype block. Hence, we subsequently screened SNPs in the genomic sequences covering *ITIH1* and *ITIH3*, except for those corresponding to repetitive sequences, by re-sequencing of genomic DNAs from 24 Japanese individuals. We identified a total of 31 SNPs and two insertion/deletion polymorphisms in *ITIH1* and 19 SNPs in *ITIH3* (Table 4). A comparison of these SNPs in the dbSNP database (The National Center for Biotechnology Information, USA) identified 9 of them (intron 2 188G > A, intron 5 646A > T, intron 15 148C > G, 299G > C, exon 19 2196G > A; R732R, 2311C > T; R771W, intron 21 327C > T in *ITIH1*; 5' flanking region –205G > A, intron 11 24C > T in *ITIH3*) to be novel as at the end of May 2006. Among the 50 SNPs we identified, we genotyped 38 SNPs with the minor allele frequencies of 10% or greater for 94 MI patients and 94 controls to construct a detailed haplotype map in this region (Fig. 1a). Using Haploview software (http://www.hapmap.org), we identified one haplotype block with four common haplotypes that covered more than 90% of the Japanese population. We selected three SNPs, rs2710322, rs2239699, and rs2286797 as tag SNPs that represented this locus (arrows, Fig. 1b) and further examined the association of each of the two additional tag SNPs (rs2710322 and rs2239699) with MI. Comparison of genotypes of 3,464 individuals with MI and 3,819 controls at these SNP loci revealed no significant association of either of the two additional SNP with MI (Table 5).

Subsequent analysis of each of the four common haplotypes against all others indicated the significant association of haplotype 4 with MI. However, since this haplotype contained the A allele for rs2286797 and the remaining haplotypes contained the G allele for it (Table 6), we considered that the haplotype association simply reflected the association of the single SNP (rs2286797).

We also investigated one SNP in *ITIH1* (intron 10 536A > C; rs3774356) that revealed strong LD with rs2286797 SNP ($r^2 = 0.93$, Fig. 1a) in the initial LD mapping. However, genotyping of the maximum number of samples at this SNP locus revealed an association with MI at a much weaker level ($\chi^2 = 19.19$, $P = 1.2 \times 10^{-5}$, comparison of allele frequency, Table 7), indicating that ITIH3 is a gene susceptible to MI.

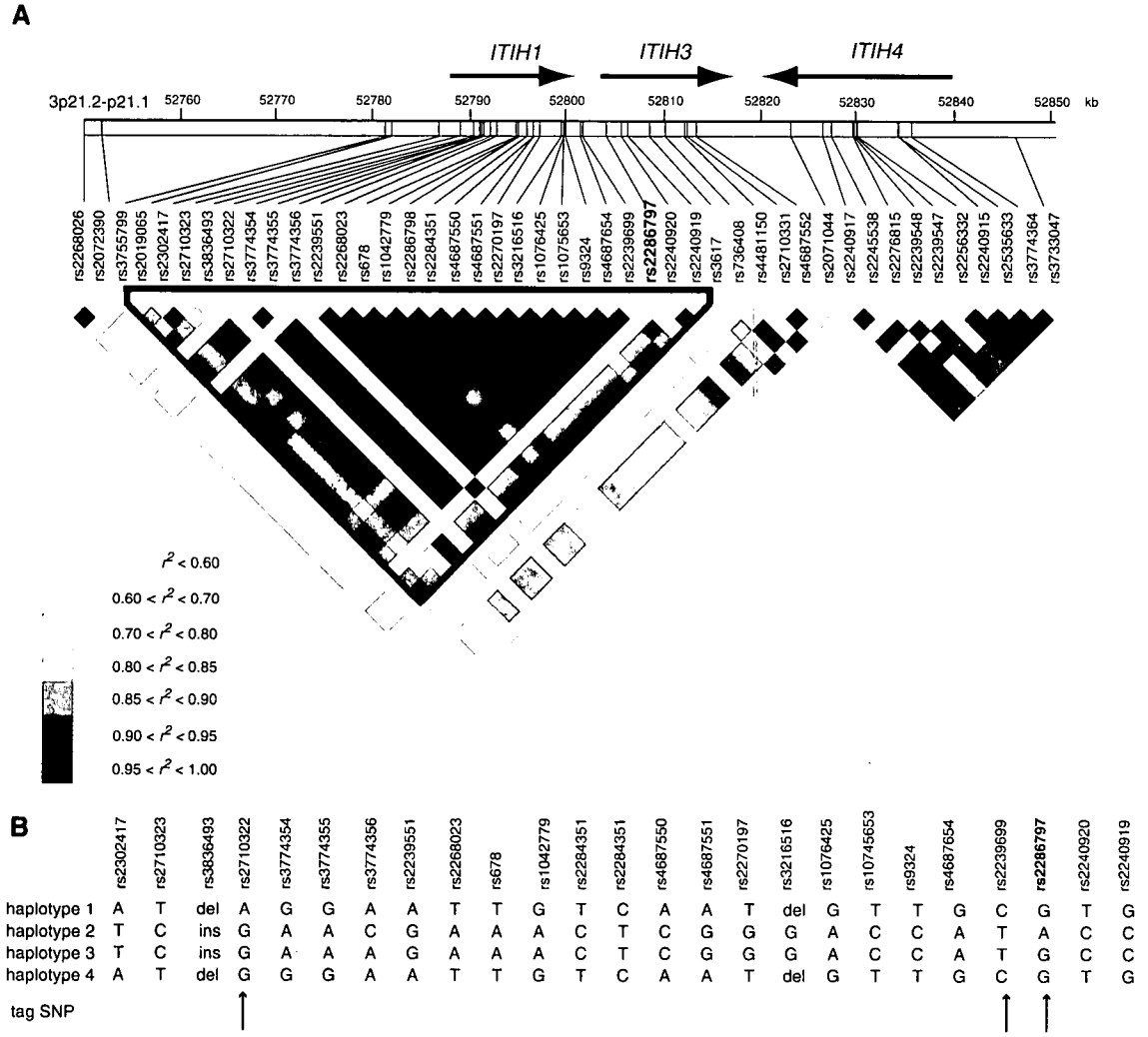

Fig. 1 Polymorphism map and haplotype structure of *ITIH1* and *ITIH3* locus. **a** Map of SNPs (MAF > 10%) in the *ITIH1* and *ITIH3* region, and pairwise LD coefficients (r^2) among them. The number of base-pair is based on genomic sequence (NC_000003.10) deposited in GenBank database. **b** Haplotype and tag SNPs in this region

Table 5 Association analysis of tag SNPs in the haplotype block

Genotype	MI (%)	CO (%)	Statistical test	Dominant model
rs2710322				
GG	1,889 (55.7)	2,107 (57.1)		
GA	1,286 (37.9)	1,349 (36.5)	χ^2	1.33
AA	216 (6.4)	236 (6.4)	*P* value	0.25
Total	3,391 (100)	3,692 (100)		
rs2239699				
CC	947 (27.9)	971 (25.7)		
CT	1,697 (50.0)	1,870 (49.5)	χ^2	7.23
TT	752 (22.1)	939 (24.8)	*P* value	0.0072
Total	3,312 (100)	3,749 (100)		

Functional analyses of the exon 2 synonymous SNP in ITIH3

Since the most statistically-significant SNP did not substitute an amino acid of ITIH3 protein, we hypothesized that this synonymous SNP affected the transcriptional regulation, because several papers reported that some transcriptional factors bound to the exonic coding sequences of some genes and regulated their transcriptional level (Mori et al. 2002; Zhang

Table 6 Haplotype association analysis using tag SNPs in the block

Haplotype ID	Case	Control	rs2710322	rs2239699	rs2286797	χ^2	*P* value
Haplotype 1	0.275	0.259	G	C	G	4.84	0.028
Haplotype 2	0.252	0.244	G	T	G	1.33	0.248
Haplotype 3	0.25	0.24	A	C	G	1.95	0.163
Haplotype 4	0.221	0.256	G	T	A	24.8	6.36×10^{-7}

Table 7 Association analysis of the SNP in *ITIH1*

Genotype	MI (%)	CO (%)	Statistical test	Allele frequency	Dominant model
rs3774356					
AA	2,035 (59.9)	2,093 (55.7)	χ^2	19.19	12.99
AC	1,194 (35.2)	1,402 (37.3)	*P* value	1.2×10^{-5}	3.1×10^{-4}
CC	166 (4.9)	261 (6.9)	Odds ratio	1.188	1.189
Total	3,395 (100)	3,756 (100)	95% CI	1.100–1.283	1.082–1.306

et al. 2004; Ikeda et al. 2005). We constructed six different reporter plasmids (Fig. 2), each of which corresponded to a genomic fragment including the SNP, and performed a luciferase assay using Jurkat and HepG2 cells. The clones containing the DNA fragment corresponding to the G allele showed greater transcriptional activity in both HepG2 and Jurkat cells than those containing the A allele (Fig. 2a, b), indicating this SNP affects transcriptional level of *ITIH3*.

Using nuclear extracts from human coronary artery smooth muscle cells (HCASMCs), human coronary artery endothelial cells (HCAECs), and Jurkat cells originated from human T lymphocyte, all of which were considered to be important players in the pathogenesis of MI, we subsequently examined the presence of some nuclear factor(s) that might bind to oligonucleotides corresponding to genomic sequences of the 108G or 108A alleles, although no known protein was predicted to bind to this DNA segment. When we used nuclear extracts from Jurkat cells (Fig. 2c), we observed two bands of different molecular weights in the lane corresponding to the G allele or the A allele, suggesting that two different nuclear proteins in Jurkat cells bound to each of the allele. However, this kind of difference was not observed when we used HCASMCs or HCAECs (data not shown).

Expression of ITIH3 protein in atherosclerotic lesion

To investigate whether ITIH3 protein was expressed in atherosclerotic plaque, we carried out immunohistochemical staining of human coronary atherectomy specimens with anti-ITIH3 antibody. As shown in Fig. 3, ITIH3 was detected in the macrophages, foam cells, and SMCs. Almost all the macrophages and foam cells were stained, some of which were aggregated around cholesterol crystals in intima. The SMCs in a deep layer of the vessel wall were stained more intensively.

Discussion

Through a large-scale, case-control association study and subsequent LD mapping, we identified *ITIH3* as a strong candidate gene conferring one of the risk factors for MI. We have demonstrated that the SNP showing the strong association with MI is likely to influence the transcriptional activity of this gene. In addition, by means of electrophoretic mobility-shift assay, we found the difference in the binding affinity to the unidentified transcription factor(s) in lymphocyte-derived cell line (Jurkat cell) in an allele-specific manner, although this difference was not observed in HCASMCs and HCAECs. Through the allele-specific difference in the ITIH3 protein level by some stress responses, T lymphocytes could contribute to the process in atherosclerotic changes through its inflammatory functions and increase the risk of MI (Libby 2002).

In addition to the in vitro experimental data, we have shown that ITIH3 protein was abundantly accumulated in SMCs and macrophages in the intima of human atherosclerotic plaques while they were absent in quiescent or normal medial SMCs, implying that ITIH3 might play a critical role in the pathogenesis of atherosclerosis and subsequent myocardial infarction.

Although functional correlation of ITIH3 with the development, progression or rupture of atherosclerotic plaques remains to be clarified, several papers reported that the members and constituents of the IαI family were detected in synovial fluid of patients with rheumatoid arthritis (Yingsung et al. 2003), in colo-

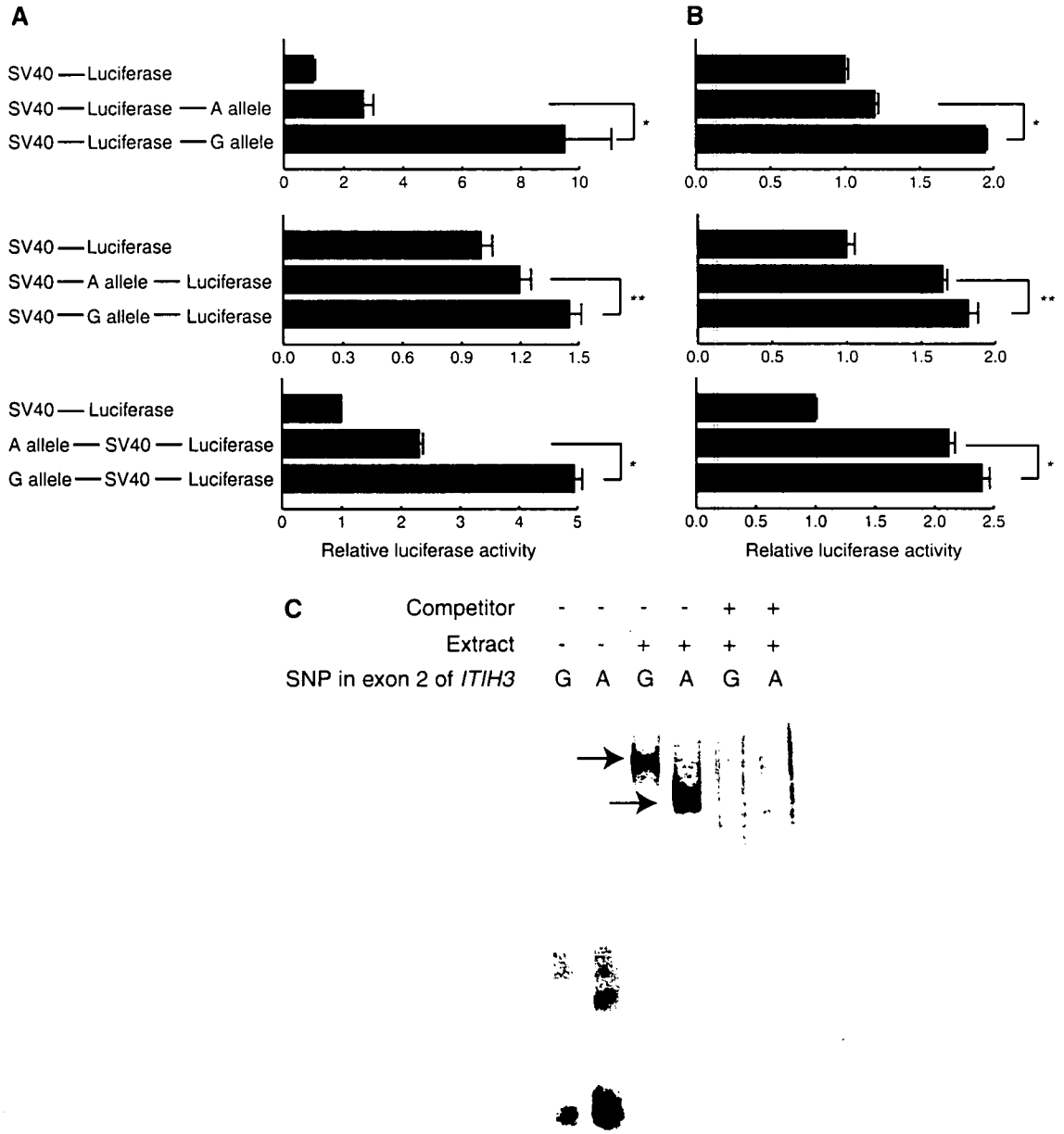

Fig. 2 Functional analyses of the SNP in exon 2 of *ITIH3* (rs2286797). Transcriptional effect by the SNP using Jurkat cells (**a**) and HepG2 cells (**b**). $^{*}P < 0.01$ and $^{**}P < 0.05$, by student's *t* test. The experiment was done in duplicate and repeated three times independently. **c** Binding of unknown nuclear factors to exon 2 of *ITIH3* in Jurkat cells. The experiment was repeated three times with similar results

rectal mucosal SMCs of patients with inflammatory bowel disease (de la Motte et al. 2003), and also in plasma of patients with sepsis (Balduyck et al. 2000), all of which suggested that they are likely to be involved in both local and systemic inflammatory response (Fries and Kaczmarczyk 2003). Furthermore, in vitro experiments revealed ITIH3 protein incorporated into the cumulus matrix through covalent linkages to HA (Zhao et al. 1995; de la Motte et al. 1999), an attachment ligand for macrophages (Ross 1999) and lymphocytes (Jean et al. 2001). Since several recent reports also suggested that genes related to inflammation conferred risk of MI (Ozaki et al. 2002, 2004, 2006; Helgadottir et al. 2004), it is conceivable that this molecule plays an important role in the pathogenesis of MI through inflammatory response.

Although the detailed biological role of ITIH3 protein in the pathogenesis of atherosclerosis is still to

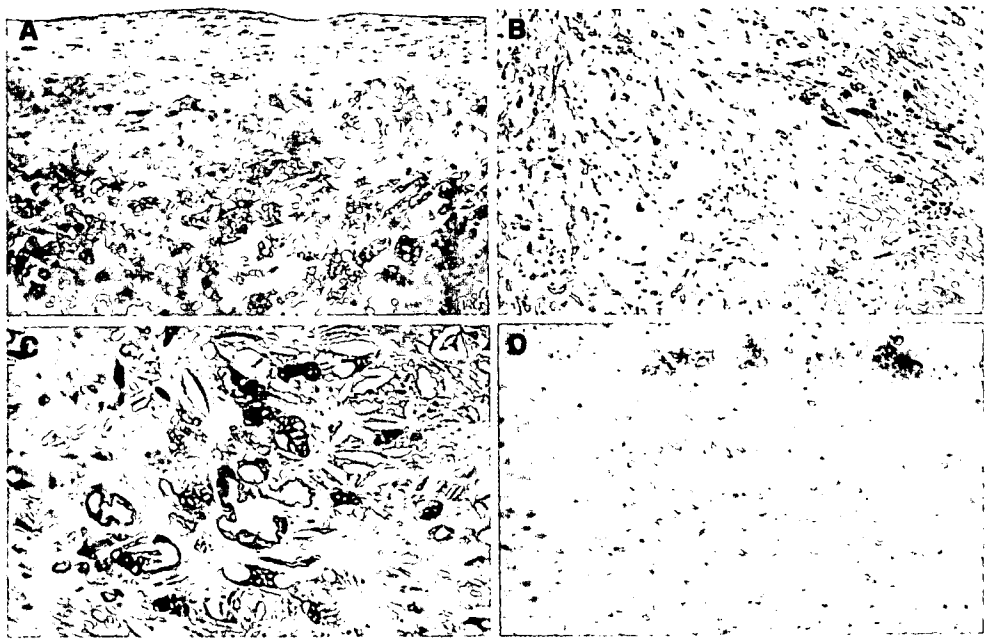

Fig. 3 Expression of ITIH3 protein in coronary atherectomy specimen. **a** Most vascular SMCs in intimal layer and macrophages in deep layer are stained. Magnification ×37. **b** Activated SMCs are migrated and proliferated in shallow layer in the vessel. Magnification ×70. **c** Foam cells aggregate around cholesterol crystals. Magnification ×70. **d** SMCs migrated from medial layer to intimal layer are stained, while those remained in medial layer are not. Magnification ×50

be clarified, we believe our findings would be an anchoring point for functional clarification of this gene and also provide a useful clue for development of novel diagnostic method, treatments and prevention for this common but serious disorder.

Acknowledgments We thank Maki Takahashi, Mayumi Yoshii, Saori Abiko, Wataru Yamanobe, Miyuki Omotezako, Yoko Ariji, Rumiko Ohishi, Makiko Watabe and Kaori Tabei and Saori Manabe for their assistance. We also thank all the other members of SNP Research Center, RIKEN and OACIS for their contribution to the completion of our study. We are also grateful to members of The Rotary Club of Osaka-Midosuji District 2660 Rotary International in Japan for supporting our study. This work was supported in part by three grants from the Takeda science foundation, the Uehara science foundation and the Japanese Millennium Project.

References

Balduyck M, Albani D, Jourdain M, Mizon C, Tournoys A, Drobecq H, Fourrier F, Mizon J (2000) Inflammtion-induced systemic proteolysis of inter-α-inhibitor in plasma from patients with sepsis. J Lab Clin Med 135:188–198

Boring L, Gosling J, Cleary M, Charo IF (1998) Decreased lesion formation in CCR2–/– mice reveals a role for chemokines in the initiation of atherosclerosis. Nature 394:894–897

Brogi E, Winkles JA, Underwood R, Clinton SK, Alberts GF, Libby P (1993) Distinct pattern of expression of fibroblast growth factors and their receptors in human atheroma and nonatherosclerotic arteries. Association of acidic FGF with plaque microvessels and macrophages. J Clin Invest 92:2408–2418

Cybulsky MI, Gimbrone MA Jr (1991) Endothelial expression of a mononuclear leukocyte adhesion molecule during atherosclerosis. Science 251:788–791

den Dunnen JT, Antonarakis SE (2000) Mutation nomenclature extensions and suggestions to describe complex mutations: a discussion. Hum Mutat 15:7–12

de la Motte CA, Hascall VC, Calabro A, Yen-Lieberman B, Strong SA (1999) Mononuclear leukocytes preferentially bind via CD44 to hyaluronan on human intestinal mucosal smooth muscle cells after virus infection or treatment with poly(I:C). J Biol Chem 274:30747–30755

de la Motte CA, Hascall VC, Drazba J, Bandyopadhyay SK, Strong SA (2003) Mononuclear leukocytes bind to specific hyaluronan structures on colon mucosal smooth muscle cells treated with polyinosinic acid; polycytidylic acid. Am J Pathol 163:121–133

Fries E, Kaczmarczyk A (2003) Inter-α-inhibitor, hyaluronan and inflammation. Acta Biochim Pol 50:735–742

Galis ZS, Sukhova GK, Lark MW, Libby P (1994) Increased expression of matrix metalloproteinases and matrix degrading activity in vulnerable regions of human atherosclerotic plaques. J Clin Invest 94:2493–2503

Haga H, Yamada R, Ohnishi Y, Nakamura Y, Tanaka T (2002) Gene-based SNP discovery as part of the Japanese Millennium Genome project; identification of 190,562 genetic variations in the human genome. J Hum Genet 47:605–610

Helgadottir A, Manolescu A, Thorleifsson G, Gretarsdottir S, Jonsdottir H, Thorsteinsdottir U, Samani NJ, Gudmundsson G, Grant SFA, Thorgeirsson G et al (2004) The gene encoding 5-lipoxygenase activating protein confers risk of myocardial infarction and stroke. Nat Genet 36:233–239

Ikeda S, Kurose K, Jinno H, Sai K, Ozawa S, Hasegawa R, Komamura K, Kotake T, Morishita H, Kamakura S et al (2005) Functional analysis of four naturally occurring variants of human constitutive androstane receptor. Mol Genet Metab 86:314–319

Ishii N, Ozaki K, Sato H, Mizuno H, Saito S, Takahashi A, Miyamoto Y, Ikegawa S, Kamatani N, Hori M, Saito S, Nakamura Y, Tanaka T (2006) Identification of a novel non-coding RNA, *MIAT*, that confers risk of myocardial infarction. J Hum Genet (in press)

Jean L, Mizon C, Larsen WJ, Mizon J, Salier J (2001) Unmasking a hyaluronan-binding site of the BX_7B type in the H3 heavy chain of the inter-α-inhibitor family. Eur J Biochem 268:544–553

Libby P (2002) Atherosclerosis in inflammation. Nature 420:868–974

Marenberg EM, Risch N, Berkman LF, Floderus B, de Faire U (1996) Genetic susceptibility to death from coronary heart disease in a study of twins. N Engl J Med 330:1041–1046

Minami M, Kume N, Shimaoka T, Kataoka H, Hayashida K, Akiyama Y, Nagata I, Ando K, Nobuyoshi M, Hanyuu M, Komeda M, Yonehara S, Kita T (2001) Expression of SR-PSOX, a novel cell-surface scavenger receptor for phosphatidylserine and oxidized LDL in human atherosclerotic lesions. Artrioscler Thromb Vasc Biol 21:1796–1800

Mori T, Anazawa Y, Iiizumi M, Fukuda S, Nakamura Y, Arakawa H (2002) Identification of the interferon regulatory factor 5 gene (IRF-5) as a direct target for p53. Oncogene 21:2914–2918

Ohnishi Y, Tanaka T, Yamada R, Suematsu K, Minami M, Fujii K, Hoki N, Kodama K, Nagata S, Hayashi T et al (2000) Identification of 187 single nucleotide polymorphisms (SNPs) among 41 candidate genes for ischemic heart disease in the Japanese population. Hum Genet 106:288–292

Ohnishi Y, Tanaka T, Ozaki K, Yamada R, Suzuki H, Nakamura Y (2001) A high-throughput SNP typing system for genome-wide association studies. J Hum Genet 46:471–477

Ozaki K, Ohnishi Y, Iida A, Sekine A, Yamada R, Tsunoda T, Sato H, Sato H, Hori M, Nakamura Y et al (2002) Functional SNPs in the lymphotoxin-α gene that are associated with susceptibility to myocardial infarction. Nat Genet 32:650–654

Ozaki K, Inoue K, Sato H, Iida A, Ohnishi Y, Sekine A, Sato H, Odashiro K, Nobuyoshi M, Hori M et al (2004) Functional variation in *LGALS2* confers risk of myocardial infarction and regulates lymphotoxin-α secretion in vitro. Nature 429:72–75

Ozaki K, Sato H, Iida A, Mizuno H, Nakamura T, Miyamoto Y, Takahashi A, Tsunoda T, Ikegawa S, Kamatani N, Hori M, Nakamura Y, Tanaka T (2006) A functional SNP in PSMA6 confers risk of myocardial infarction in the Japanese population. Nat Genet 38:921–225

Ross R (1999) Atherosclerosis—an inflammatory disease. N Engl J Med 340:115–126

Shea S, Ottman R, Gabrieli C, Stein Z, Nichols A (1984) Family history as an independent risk factor for coronary artery disease. J Am Coll Cardiol 4:793–801

Storey JD (2002) A direct approach to false discovery rate. J R Stat Soc Ser B 64:479–498

The International HapMap Consortium (2003) The International HapMap Project. Nature 426:789–796

Tsunoda T, Lathrop GM, Sekine A, Yamada R, Takahashi A, Ohnishi Y, Tanaka T, Nakamura Y (2004) Variation of gene-based SNPs and linkage disequilibrium patterns in the human genome. Hum Mol Genet 13:1623–1632

Wang Q, Rao S, Shen GQ, Li L, Moliterno DJ, Newby LK, Rogers WJ, Cannata R, Zirzow E, Elston RC et al (2004) Premature myocardial infarction novel susceptibility locus on chromosome 1p34–36 identified by genomewide linkage analysis. Am J Hum Genet 74(2):262–271

Yamada R, Tanaka T, Unoki M, Nagai T, Sawada T, Ohnishi Y, Tsunoda T, Yukioka M, Maeda A, Suzuki K et al (2001) Association between a single-nucleotide polymorphism in the promoter of the human interleukin-3 gene and rheumatoid arthritis in Japanese patients, and maximum-likelihood estimation of combinatorial effect that two genetic loci have on susceptibility to the disease. Am J Hum Genet 68:674–685

Yamada Y, Izawa H, Ichihara S, Takatsu F, Ishihara H, Hirayama H, Sone T, Tanaka M, Yokota M (2002) Prediction of the risk of myocardial infarction from polymorphisms in candidate genes. N Engl J Med 347:1916–1923

Yingsung W, Zhuo L, Morgelin M, Yoneda M, Kida D, Watanabe H, Ishiguro N, Iwata H, Kimata K (2003) Molecular heterogeneity of the SHAP-hyaluronan complex. J Biol Chem 278:32710–32718

Zhang EY, Fu DJ, Pak YA, Stewart T, Mukhopadhyav N, Wrighton SA, Hillgeren KM (2004) Genetic polymorphisms in human proton-dependent dipeptide transporter PEPT1: implications for the functional role of Pro586. J Pharmacol Exp Ther 310(2):437–445

Zhao M, Yoneda M, Ohashi Y, Kurono S, Iwata H, Ohnuki Y, Kimata K (1995) Evidence for the covalent binding of SHAP, heavy chains of inter-α-trypsin inhibitor, to hyaluronan. J Biol Chem 270:26657–26663

Zhuo L, Hascall VC, Kimata K (2004) Inter-α-trypsin inhitibor, a covalent protein-glycosaminoglycan-protein complex. J Biol Chem 279:38079–38082

Available online at www.sciencedirect.com
ScienceDirect
Journal of Molecular and Cellular Cardiology 42 (2007) 662–669
Journal of Molecular and Cellular Cardiology
www.elsevier.com/locate/yjmcc

Original article

Mechanistic basis for the pathogenesis of long QT syndrome associated with a common splicing mutation in KCNQ1 gene

Keiko Tsuji [a,c,d], Masaharu Akao [a,*], Takahiro M. Ishii [b], Seiko Ohno [a], Takeru Makiyama [a], Kotoe Takenaka [a], Takahiro Doi [a], Yoshisumi Haruna [a], Hidetada Yoshida [a], Toshihiro Nakashima [c], Toru Kita [a], Minoru Horie [d]

[a] *Department of Cardiovascular Medicine, Kyoto University Graduate School of Medicine, 54 Kawahara-cho, Shogoin, Sakyo-ku, Kyoto 606-8507, Japan*
[b] *Department of Physiology, Kyoto University Graduate School of Medicine, Japan*
[c] *Department of Applied Biology, Kyoto Institute of Technology, Kyoto, Japan*
[d] *Department of Cardiovascular and Respiratory Medicine, Shiga University of Medical Science, Japan*

Received 22 September 2006; received in revised form 15 December 2006; accepted 28 December 2006
Available online 5 January 2007

Abstract

Mutations in KCNQ1, the gene encoding the delayed rectifier K^+ channel in cardiac muscle, cause long QT syndrome (LQTS). We studied 3 families with LQTS, in whom a guanine to adenine change in the last base of exon 7 (c.1032G>A), previously reported as a common splice-site mutation, was identified. We performed quantitative measurements of exon-skipping KCNQ1 mRNAs caused by this mutation using real-time reverse transcription polymerase chain reaction. Compared with normal individuals who have minor fractions of splicing variants (Δ7–8: 0.1%, Δ8: 6.9%, of total KCNQ1 transcripts), the affected individuals showed remarkable increases of exon-skipping mRNAs (Δ7: 23.5%, Δ7–8: 16.8%, Δ8: 4.5%). Current recordings from *Xenopus laevis* oocytes heterologously expressing channels of wild-type (WT) or exon-skipping KCNQ1 (Δ7, Δ7–8, or Δ8) revealed that none of the mutants produced any measurable currents, and moreover they displayed mutant-specific degree of dominant-negative effects on WT currents, when co-expressed with WT. Confocal microscopy analysis showed that fluorescent protein-tagged WT was predominantly expressed on the plasma membrane, whereas the mutants showed intracellular distribution. When WT was co-expressed with mutants, the majority of WT co-localized with the mutants in the intracellular space. Finally, we provide evidence showing direct protein–protein interactions between WT and the mutants, by using fluorescence resonance energy transfer. Thus, the mutants may exert their dominant-negative effects by trapping WT intracellularly and thereby interfering its translocation to the plasma membrane. In conclusion, our data provide a mechanistic basis for the pathogenesis of LQTS caused by a splicing mutation in KCNQ1.

Keywords: Potassium channels; Arrhythmia; Long QT syndrome; Mutation; Splicing

1. Introduction

Long QT syndrome (LQTS) is characterized by prolongation of the cardiac action potential, syncopal attacks, torsades de pointes arrhythmias, and sudden cardiac death [1–3]. The slow component of delayed rectifier K^+ current (I_{Ks}) in the heart modulates repolarization of cardiac action potential. The I_{Ks} channel is formed by the co-assembly of KCNQ1 α-subunits and KCNE1 β-subunits [4,5]. Mutations in the KCNQ1 cause the most frequent form of inherited LQTS [6]. We studied 3 families with LQTS, in whom a guanine to adenine change in the last base of exon 7 (c.1032G>A) of KCNQ1 was identified. Among our entire group of KCNQ1-related LQTS patients, the frequency of this mutation was remarkably high (we found this mutation in 3 out of 22 families with KCNQ1 mutations, among a total of 185 families with LQTS), in agreement with the previous report that this is a mutation "hot-spot" [7]. Mutations at this spot (c.1032G>A or c.1032G>C), which do not alter the coded alanine (A344A), have been considered to act as splice mutations in KCNQ1, by altering the intron 7 donor splice-site consensus sequence [8,9]. Murray et al. [7] demonstrated the presence of exon-skipping transcripts (with loss of exon 8 (Δ8) or of exon 7–8 (Δ7–8)) in peripheral blood leukocytes of

* Corresponding author. Tel.: +81 75 751 3194; fax: +81 75 751 4284.
E-mail address: akao@kuhp.kyoto-u.ac.jp (M. Akao).

0022-2828/$ - see front matter © 2007 Elsevier Inc. All rights reserved.
doi:10.1016/j.yjmcc.2006.12.015

affected individuals, using reverse transcription polymerase chain reaction (RT-PCR). Given the high frequency of this mutation among LQTS patients, elucidating the detailed molecular mechanisms by which this mutation affects the phenotypes of LQTS is of critical importance.

Pre-mRNA processing is an important aspect of gene expression and consists of the precise recognition of exons and removal of introns in such a way that the exons are joined to form mature mRNAs with intact translational reading frames [10,11]. Disruption of normal splicing as a result of genetic mutation can lead to the generation of abnormal proteins or the degradation of aberrant transcripts through nonsense-mediated decay, and thus to the pathogenesis of a variety of human diseases [12].

The present study was therefore designed to understand the molecular basis of the pathogenesis of LQTS caused by this relatively common splicing mutation in the KCNQ1 gene. We carried out quantitative analysis of exon-skipping transcripts of the KCNQ1 gene using real-time RT-PCR and examined how those quantitative changes may contribute to the pathogenesis using a variety of biochemical and biophysical approaches: voltage-clamp current recordings, confocal microscopy, and fluorescence resonance energy transfer (FRET) analysis.

2. Materials and methods

2.1. Genomic DNA isolation and mutation analysis

Mutation analysis was carried out as previously described [13] with our minor modifications. Genomic DNA was prepared from peripheral blood leukocytes using QIAamp DNA Blood Midi Kits (Qiagen: Valencia, CA). 16 exons of the KCNQ1 gene were amplified by PCR using intronic primer sequences. Genetic screening was performed for KCNQ1 by denaturing high-performance liquid chromatography (DHPLC) using a WAVE System Model 3500 (Transgenomic: Omaha, NE). Abnormal conformers were amplified by PCR and sequencing was performed on an ABI PRISM3100 DNA sequencer (Applied Biosystems: Foster City, CA). We also carried out a complete screening for other LQTS-causing genes; KCNH2, SCN5A, KCNE1, and KCNJ2.

2.2. RNA extraction and real-time RT-PCR

Total RNA was extracted from leukocytes of fresh blood using QIAamp RNA Blood Mini Kits (Qiagen). Subsequently, DNase-treated total RNA was reverse-transcribed by use of the SuperScriptIII FirstStrand Synthesis System (Invitrogen: Carlsbad, CA) and was used as a template for subsequent PCR reactions. We used the exon 5-F forward primer (5′-GGGCATC-CGCTTCCTGCAGA-3′) and the exon 10-R reverse primer (5′-CCATTGTCTTTGTCCAGCTTGAAC-3′) to amplify KCNQ1 cDNA from exons 5 through 10.

Measurements of normal and mutant mRNA levels were performed by real-time RT-PCR by use of an ABI PRISM 7900HT Sequence Detection System (Applied Biosystems). The reaction mixture contained SYBR Green PCR Master Mix (Applied Biosystems), cDNA template, and PCR primers. In order to selectively amplify these splicing variants, PCR primers were designed so that they spanned the adjacent exons: Exon 6.8-F: 5′-CTGTGGTGGGGGGTG-GGGATT-3′, Exon 6.9-F: 5′-TGTGGTGGGGGGTG-ACCGCAT-3′, Exon 7.9-F: 5′-CTTT-GCGCTCCCAGCG-ACCG-3′ (all the hyphens inside the primer sequence indicate the boundaries of exons). In all cases, the dissociation curves showed that there was no significant contribution of relatively short by-products to the measured fluorescence intensities.

All the samples were tested in duplicate. A standard curve for each primer pair was obtained using serial dilutions of a recombinant plasmid containing cDNA. The threshold cycle (Ct) was subsequently determined. Relative mRNA levels of splice mutants were calculated based on the Ct values and normalized by the GAPDH level of each sample. The amounts of mutant cDNA were expressed as a percentage of the total KCNQ1 mRNA, for which exons 9 through 10 were amplified with the exon 9-F forward primer (5′-CGCATGGAGGTGC-TATGCT-3′) and the exon 10-R reverse primer.

2.3. Oocyte isolation and electrophysiology

Xenopus laevis oocytes were prepared and current recordings were carried out as described previously [14]. Each KCNQ1 cRNA (10 ng) alone or wild-type (WT) cRNA (10 ng) plus mutant-cRNA (10 ng) was injected into *Xenopus* oocytes. All the current recordings in the present study were performed in the presence of KCNE1 β-subunits (1 ng). Background I_{Ks} current was recorded in oocytes injected with KCNE1 alone.

An axoclamp-2B amplifier (Axon Instruments, Union City, CA) was used to record currents at 25 °C in oocytes 4–5 days after cRNA injection, using standard two-electrode voltage-clamp techniques. To decrease the interference from endogenous Cl^- current, we used a low-Cl^- bath solution (mM): NaOH 96, KOH 2, $CaCl_2$ 2, $MgCl_2$ 1, MeS 101, HEPES 5 (pH titrated to 7.6 with methanesulfonic acid). Currents were sampled at 10 kHz and filtered at 2 kHz. Voltage steps were applied with 3-s pulses in 10 mV increments from a holding potential of −80 mV to voltages from −70 to +60 mV, and then to −30 mV, where tail currents were recorded. Current amplitudes were measured at 1.5-s after the initiation of 3-s pulse applied to a +50 mV test potential, followed by the subtraction of background I_{Ks} current (49.5 nA).

2.4. Cell preparation and confocal imaging

For confocal microscopy experiments, green fluorescent protein (GFP)-tagged KCNQ1 was constructed using EGFP-N1 vector (Clontech: Mountain View, CA). COS7 cells were plated on 35-mm glass-bottom culture dishes and maintained for 12–24 h in Dulbecco's modified Eagle's medium containing 20% FBS. Lipofection was performed with Lipofectamine reagent (Invitrogen). 48 h after transfection, COS7 cells were incubated for 24 h with 100 μM cycloheximide. The localization of GFP-tagged proteins was detected using a Zeiss laser-scanning confocal microscope (Zeiss LSM510 META) with a 63 × 1.40

numerical aperture oil-immersion objective. GFP was excited using a 488-nm line of an argon laser and signals were collected through a 500–530 band-pass filter.

2.5. FRET

FRET imaging has been proven to be a powerful tool for detecting protein–protein interactions in living cells [15]. We used a FRET experiment protocol with acceptor photobleaching and spectral unmixing [16] with minor modifications. We constructed cyan or yellow fluorescent protein (CFP, YFP)-tagged KCNQ1 using ECFP-C1 or EYFP-C1 vector (Clontech), respectively. FRET was measured by acceptor photobleaching, where an increase in CFP signal (dequenching) during incremental photobleaching of YFP can be observed. Samples were excited with a 458-nm line of an argon laser, and confocal images were obtained before and after acceptor photobleaching (a 514-nm line of an argon laser was used to photobleach YFP), by using a 458- to 514-nm dichroic beamsplitter, and the META detector was set between 473 and 558 nm. The two temporally averaged 3D image sets (x, y and spectrum) were linearly unmixed, resulting in four 2D fluorescence data sets (the donor/acceptor before/after photobleaching). Finally, subtracting the unmixed donor emission before the photobleaching from that after photobleaching resulted in the net FRET distribution. FRET efficiency (E) was calculated as:

$$E = \frac{I_D - I_{DA}}{I_{DA}}(\%),$$

where I_{DA} is the CFP-normalized fluorescence intensity before and I_D is the CFP-normalized fluorescence intensity after photobleaching of the acceptor (YFP).

2.6. Statistical analysis

Quantitative data are presented as the mean ± SEM. Multiple comparisons among groups were carried out by one-way ANOVA with Bonferroni's least significant difference as the post hoc test. A level of $p<0.05$ was accepted as statistically significant.

3. Results

3.1. Mutation analysis

Pedigrees and the clinical features for the 3 LQTS families (Family K176, K214 and K155) examined in this study are shown in Supplementary Figure. The 3 families were unrelated. DNA samples from 8 members of the families (II-6, III-2, III-3, IV-1, IV-2 in Family K176, III-1 in Family K214, and I-1, II-1 in Family K155) were subjected to a mutation screening of the KCNQ1 gene. An abnormal migration pattern was identified by DHPLC analysis (Fig. 1, left panel; note the comparable height of the left and right peaks) in KCNQ1 exon 7 of the 6 affected individuals (II-6, III-2, III-3 in Family K176, III-1 in Family K214, and I-1, II-1 in Family K155). The remaining 2 individuals

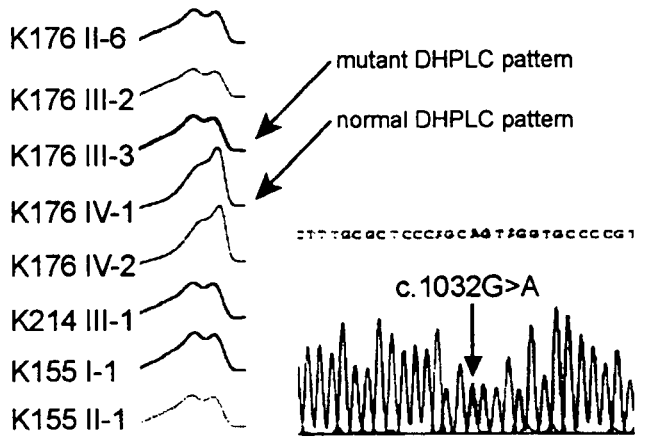

Fig. 1. Mutation analysis. Left panel: DHPLC revealed abnormal migration patterns in the affected individuals. Right panel: Automated DNA sequencing electropherogram demonstrates c.1032G>A mutation.

(IV-1, IV-2 in K176) showed normal patterns, as indicated by the greater height of the right peak (Fig. 1, left panel). DNA sequencing identified a heterozygous guanine to adenine change in KCNQ1 at nucleotide 1032 (c.1032G>A) (Fig. 1, right panel), which is the last base of exon 7. Among our entire group of KCNQ1-related LQTS patients, the frequency of this mutation was remarkably high (we found this mutation in 3 out of 22 families with KCNQ1 mutations, among a total of 185 families with LQTS). We ruled out the presence of mutations in other LQTS-causing genes (KCNH2, SCN5A, KCNE1, and KCNJ2).

3.2. Identification of exon-skipping KCNQ1 mRNAs using RT-PCR

To directly show the presence of exon-skipping transcripts, a total RNA sample from the proband of Family K176 was subjected to RT-PCR (Fig. 2a), using primers spanning exons 5 through 10. RNA samples were available only from the family. In contrast with the single WT band identified in normal individuals, the affected individual had shorter bands as well as the normal-sized WT. The direct sequencing of these short-sized transcripts revealed the existence of three kinds of exon-skipping mRNAs (Δ7–8:399 bp, Δ7: 495 bp, Δ8: 510 bp, WT: 606 bp). The previous report identified Δ8 and Δ7–8 mRNAs (referred as Δ7 and Δ6–7 in this report) [7], but we additionally identified Δ7 mRNA in this study. Fig. 2b shows a schematic structure of KCNQ1 channel subunit. Similar to other voltage-gated K^+ channel α-subunits, the KCNQ1 protein has six transmembrane domains (S1–S6), a voltage sensor (S4) and a pore helix selectivity filter segment (P-loop) that connects S5 and S6. Exon 7 spans from part of the P-loop to part of the S6 region. Exon 8 constitutes the rest of S6 and part of the intracellular C-terminal domain.

3.3. Quantification of exon-skipping KCNQ1 mRNAs using real-time RT-PCR

We carried out quantitative analysis of short-sized mutant mRNAs in 3 affected members of Family K176, using real-time

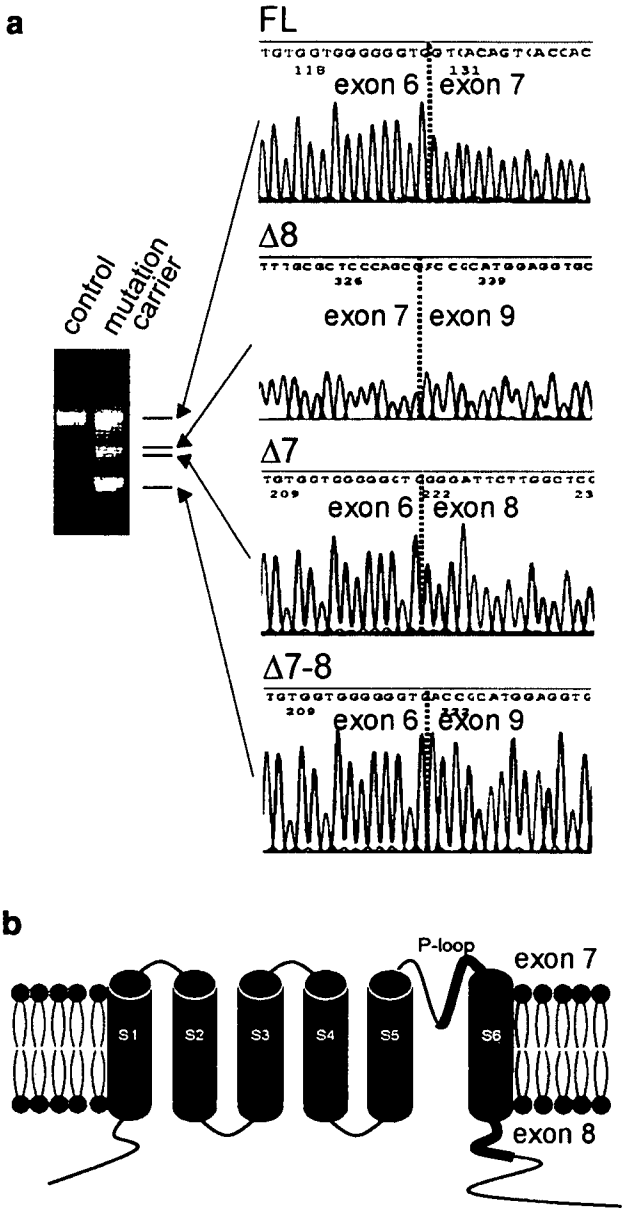

Fig. 2. Identification of exon-skipping mRNAs using RT-PCR. (a) RT-PCR from lymphocytes of a control and a mutation carrier. Nucleotide sequence of each of the exon-skipping mRNAs is also shown. (b) Scheme of the transmembrane topology of the cardiac KCNQ1 channel illustrating the location of the mutation (red asterisk) and that of exons 7 (green) and 8 (blue). The cardiac KCNQ1 channel α-subunit consists of 6 transmembrane-spanning segments (S1 through S6), and S5 and S6 are connected by the P-loop.

RT-PCR. In order to selectively amplify these splicing variants, PCR primers were designed so that they spanned the adjoining exons (Fig. 3a). Fig. 3b shows a representative amplification plot of Δ7–8 for controls (n=4), mutation carriers (n=3) and no template control, indicating the increases of the Δ7–8 mRNA in mutation carriers. Compared with normal individuals who had minor fractions of splicing variants (WT: 93.0±0.7%, Δ7: 0.0±0.0%, Δ7–8: 0.1±0.0%, Δ8: 6.9±0.7%, of total KCNQ1 transcripts; n=4), the affected individuals showed significant increases of exon-skipping mRNAs (WT: 55.2± 0.9%, Δ7: 23.5±1.7%, Δ7–8: 16.8±0.9%, Δ8: 4.5±0.7%; n=3) (Fig. 3c).

3.4. Biophysical characteristics of exon-skipping KCNQ1 proteins

Electrophysiological properties of mutant KCNQ1 proteins were characterized in *X. laevis* oocytes injected with cRNA of WT or mutants (Δ7, Δ7–8, Δ8) (Fig. 4). In the *Xenopus* oocytes injected with WT, depolarizing pulses evoked time-

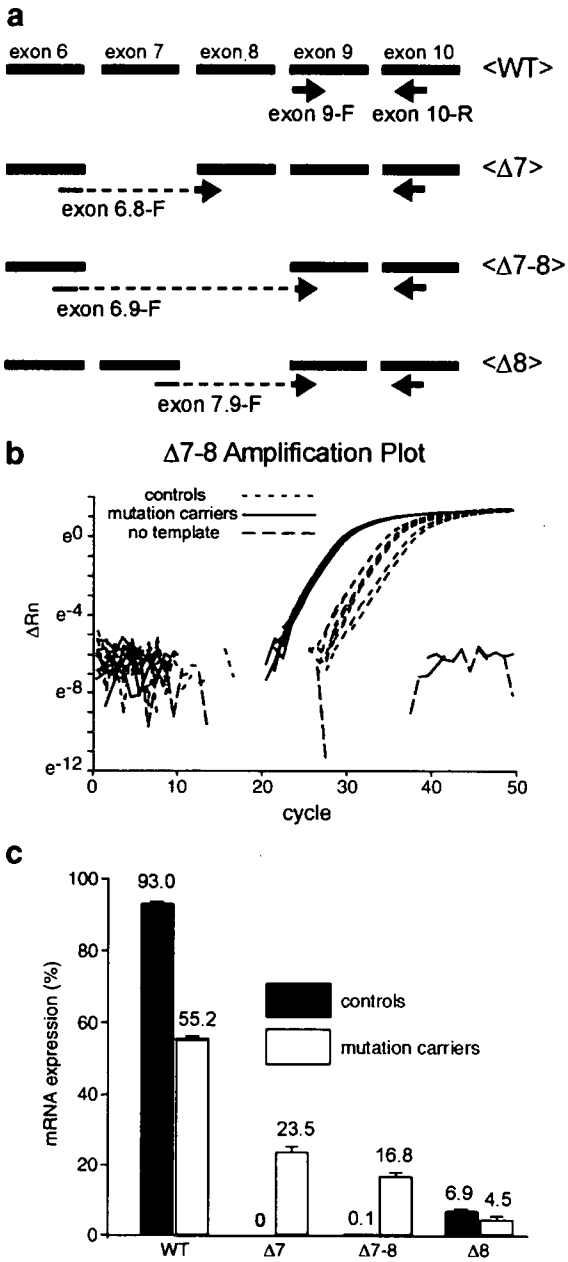

Fig. 3. Real-time RT-PCR analysis. (a) Scheme of the real-time PCR primers used to quantify the splicing mutants. A common reverse primer, exon 10-R located in exon 10, was used. Specific amplification of each splice mutant was performed with specific forward primers spanning the adjacent exons: exon 6.8-F primer for Δ7 mRNA, exon 6.9-F primer for Δ7–8 mRNA, and exon 7.9-F primer for Δ8 mRNA. (b) Representative amplification plot of Δ7–8 in real-time PCR analysis, indicating the increases of the Δ7–8 mRNA in mutation carriers. (c) Percentages of WT and mutant mRNAs. The amounts of mutant mRNA were expressed as a percentage of the total KCNQ1 mRNA. Data are the mean±SEM. Controls: 4 normal healthy individuals. Mutation carriers: 3 members of Family K176.

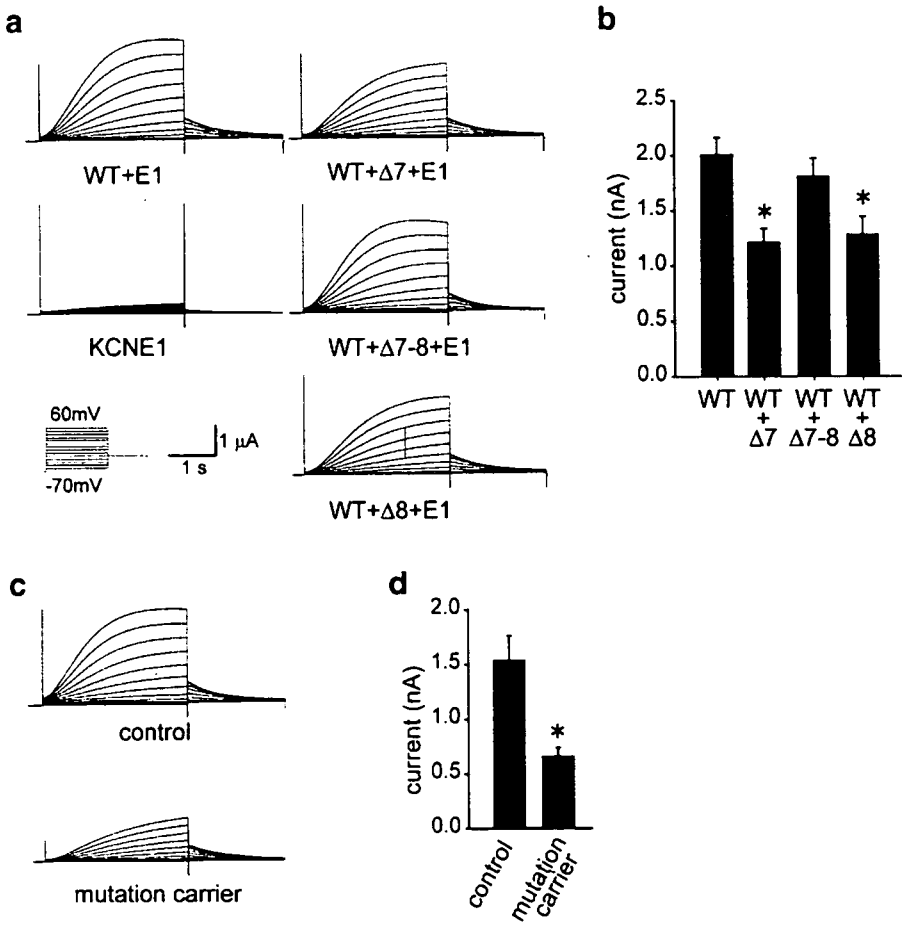

Fig. 4. Electrophysiological analysis. (a) Representative current traces recorded from two-electrode voltage-clamp of *X. laevis* oocytes heterologously expressing channels of WT or exon-skipping KCNQ1. Currents were recorded at various membrane potentials from −70 to +60 mV for 3 s in 10 mV increments from a holding potential of −80 mV. WT: 10 ng of WT cRNA was injected. WT+mutant (either Δ7, Δ7–8 or Δ8): 10 ng of WT plus 10 ng of mutant cRNA. All the current recordings in the present study were performed in the presence of KCNE1 β-subunits (1 ng). Background I_{Ks} current was recorded in oocytes injected with KCNE1 alone. (b) Pooled data of currents. Current amplitudes were measured at 1.5 s after the initiation of 3-s pulse applied to a +50 mV test potential. Background I_{Ks} current (49.5 nA) was subtracted. $n=8$ for WT, 8 for WT+Δ7, 8 for WT+Δ7–8, and 11 for WT+Δ8. *$p<0.01$ vs. WT. (c) Representative current traces recorded from oocytes simulating the proportions of mRNA of control individuals and mutation carriers. A total of 10 ng of cRNA was injected with the relative ratios of WT and mutant KCNQ1 inferred from the data obtained in the real-time RT-PCR experiment. (d) Pooled data of currents. $n=6$ for control, and 6 for mutation carriers. *$p<0.01$ vs. control.

dependent outward currents, indicating typical I_{Ks} channel properties (Fig. 4a, upper left panel). Background I_{Ks} current obtained in oocytes injected with KCNE1 alone was small (49.5 nA) (Fig. 4a, lower left panel). The *Xenopus* oocytes injected with Δ7, Δ7–8, or Δ8 alone displayed no time-dependent currents (data not shown), indicating that these mutants are non-functional.

To assess the functional interaction between WT and mutant channels, we co-expressed WT cRNA (10 ng) plus either one of the mutant cRNA (10 ng). The activated current amplitude of WT was 2.01±0.15 μA ($n=11$) (Figs. 4a, b). The current amplitudes with WT plus mutant KCNQ1 were recorded, and some of them were significantly smaller than those of WT (WT+Δ7: 1.22±0.12 μA, $n=8$, $p<0.01$; WT+Δ7–8: 1.82±0.16 μA, $n=8$, $p=0.34$; WT+Δ8: 1.29±0.16 μA, $n=11$, $p<0.01$) (Figs. 4a, b). These data clearly show that each exon-skipping KCNQ1 protein had the mutant-specific level of dominant-negative effect on WT channels.

In order to simulate the electrophysiological properties of cardiac cells of the affected patients, we injected the cRNAs (total 10 ng) with the relative ratios of WT and mutant KCNQ1 inferred from the data obtained in the real-time RT-PCR experiment. Cells with the cRNA ratios of the patients showed pronounced reduction in currents compared with those with the ratios of normal individuals; 1.55±0.22 μA ($n=6$) for control, 0.67±0.08 μA ($n=6$) for mutation carriers ($p<0.01$) (Figs. 4c, d). This profound suppression of I_{Ks} current may underlie the pathophysiology of these patients.

3.5. Subcellular localization of exon-skipping KCNQ1 proteins

To further explore the molecular basis of the dominant-negative effects of exon-skipping KCNQ1 proteins, we examined the subcellular localization using GFP-tagged KCNQ1 heterologously expressed in COS7 cells (Fig. 5). WT-GFP (Fig. 5a) appeared to be expressed on the plasma membrane

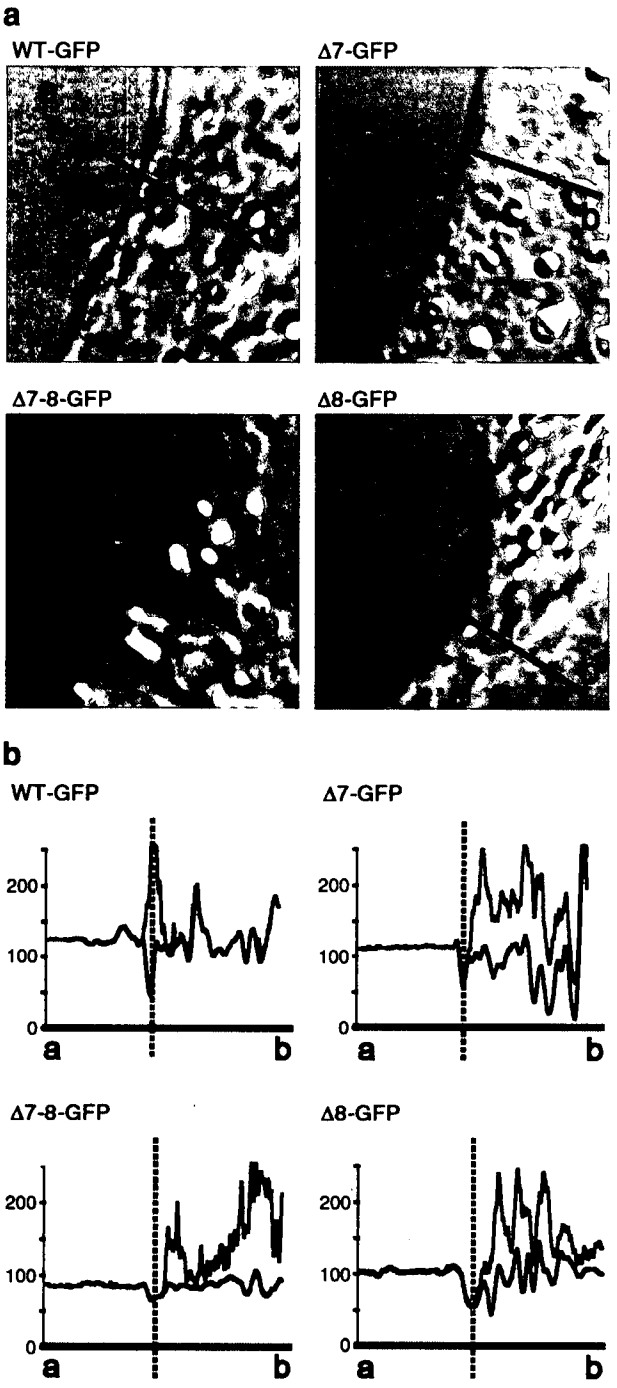

Fig. 5. Confocal microscopy analysis. (a) Overlay of transmitted bright-field image (gray) and GFP fluorescence image (green). (b) Line profile of pixel intensities (black: bright field; green: GFP) from the a-b line drawn in panel a. Vertical dashed lines represent the position of the plasma membrane. These results were representative ones obtained from at least three independent experiments.

(upper left); overlay with bright-field image (gray scale) showed green fluorescence along the plasma membrane. In the line profiles (Fig. 5b), the first major deflection in the black lines (bright-field) was defined as the plasma membrane (as indicated by the dashed vertical lines). WT-GFP had a peak at the level of the plasma membrane. In contrast, all of the mutants were retained in the cytoplasmic compartment, and GFP peaks appeared inside the cell, but not on the level of the plasma membrane (Fig. 5). These data clearly indicate that mutant KCNQ1 proteins were unable to translocate to the plasma membrane.

3.6. Direct interaction between WT and exon-skipping KCNQ1 proteins

The dominant-negative effects of the mutants suggest that they may suppress the trafficking of the WT channel to the plasma membrane. We examined this possibility by employing the co-expression of WT-YFP and Δ7-CFP (Fig. 6a). WT, which was predominantly expressed on the plasma membrane when expressed alone (data not shown, but see Fig. 5a), was retained in the intracellular compartment with remarkably reduced plasma membrane expression in the presence of Δ7. Furthermore, WT-YFP co-localized with Δ7-CFP, as shown in the merged image (Fig. 6a, upper three panels).

We then performed the FRET experiment with the acceptor bleaching method to detect the direct interaction between WT and mutant KCNQ1 subunits. The increase in CFP fluorescence intensity after YFP bleaching (Fig. 6a, lower panels) indicates that Δ7 physically interacted with the WT subunit in an intracellular compartment and prevented it from translocating into the plasma membrane.

Fig. 6b shows the summarized data regarding FRET efficiency. As for negative controls, we employed WT-CFP alone (second-to-the-right bar) and CFP plus YFP (the right-most bar). The FRET efficiency between WT and all the mutants was significantly larger than that of the negative controls ($^{*}p<0.05$ vs. WT-CFP, $^{\#}p<0.05$ vs. CFP plus YFP). Hence, all of the mutants showed the mutant-specific degree of direct interaction with the WT subunit.

4. Discussion

We performed biochemistry, electrophysiology, and cellular imaging studies to examine the behavior of WT and mutant channel subunits created by the relatively common KCNQ1 splicing mutation and provided deeper mechanistic insights into the pathogenesis of LQTS caused by this mutation.

4.1. Generation of exon-skipping KCNQ1 mRNAs

In eukaryotic cells, removal of introns from pre-mRNAs by pre-mRNA splicing is an essential process for gene expression [10,17]. Splicing is a tightly-regulated part of RNA processing, and its abnormality caused by somatic mutations can result in the production of abnormal proteins and cause a variety of human diseases [12]. Here, we studied 3 LQTS families, in whom a G to A change in the last base of exon 7 (c.1032G>A) was identified. This mutation was previously reported to alter the donor splice-site of intron 7, resulting in the production of exon-skipping transcripts, but not to alter the coded alanine (A344A) [7–9], since it involves the characteristic consensus sequence of the splicing donor site, A*G*/GUAAGU. *G* at this position is reportedly present in 78% of exons of various genes,

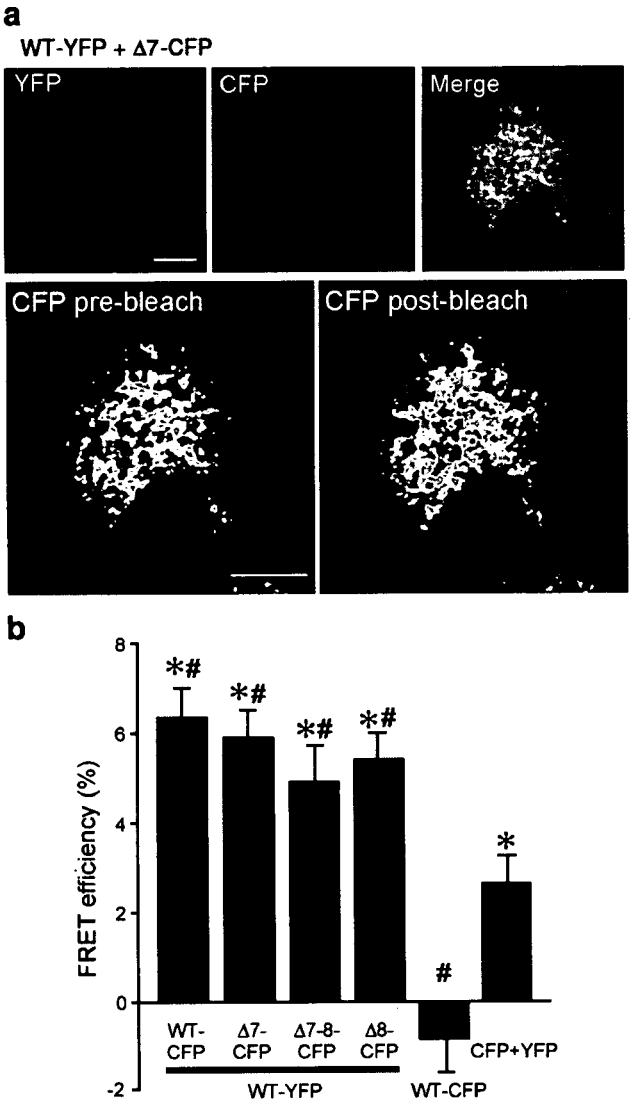

Fig. 6. FRET analysis. (a) WT-YFP and Δ7-CFP were co-expressed in COS7 cells. WT-YFP is pseudocolored in red (left panel) and Δ7-CFP is pseudocolored in green (middle panel). The merged image in the right panel shows co-localization of Δ7-CFP and WT-YFP. Scale bar: 10 μm. (b) Pseudocolor images of Δ7-CFP before (CFP pre-bleach) and after (CFP post-bleach) YFP photobleaching. (c) Summarized data of FRET efficiency. $^{*}p<0.05$ vs. WT-CFP, $^{\#}p<0.05$ vs. CFP+YFP.

and its mutations are responsible for several human diseases, such as Ehlers–Danlos syndrome, Tay–Sachs disease, acute intermittent porphyria, and β-thalassemia [18–21].

Using RT-PCR, we initially confirmed the presence of several short-sized exon-skipping mRNAs (Δ7, Δ7–8, and Δ8) as well as the normal-sized one in peripheral blood lymphocytes from the affected individuals (Fig. 2a). The presence of Δ7–8 and Δ8 mRNAs was previously reported in patients with this mutation [7], but we newly identified a functionally important mutant, Δ7 mRNA, in the present study. We quantitatively showed significant increases of exon-skipping mRNAs (Δ7 and Δ7–8) in the affected individuals compared with normal individuals, who have minor fractions of splicing variants (mostly Δ8), using real-time RT-PCR (Fig. 3c). Interestingly, the mutation at the intron 7 donor splice-site not only affected the binding between exons 7 and 8 but also had significant effects on the binding of exons remote from the mutation: exons 8 and 9, and exons 6 and 9. This observation is noteworthy, considering the fact that splicing mutations are rarely associated with multiple exon skipping [22,23]. Wijk et al. [24] reported a similar case demonstrating the presence of Δ5 and Δ5–6 caused by an intron 5 donor splice-site mutation in the PKLR gene in a patient with pyruvate kinase deficiency. The splice-site recognition of exons may therefore depend on the neighboring exons or introns; the presence of exonic (or intronic) splicing enhancers or silencers in the vicinity of the donor splice-site and acceptor splice-site motifs [25,26] may be involved in our aberrant KCNQ1 splicing, but further studies are needed to prove this hypothesis.

4.2. Functional characterization of exon-skipping KCNQ1 proteins

In the following set of experiments, we aimed to determine the functional characteristics of exon-skipping mutant proteins and to examine their interaction with WT proteins, using electrophysiological and cellular imaging techniques. Current recordings in *Xenopus* oocytes heterologously expressing channels composed of WT or splicing mutant (Δ7, Δ7–8 and Δ8) proteins showed that none of the mutant channels produced measurable currents, and moreover all the mutant proteins displayed the mutant-specific level of dominant-negative effects on WT currents, when co-expressed with WT (Figs. 4a, b).

Confocal microscopy analyses showed that the mutant proteins were retained in an intracellular compartment (presumably, endoplasmic reticulum) and were unable to translocate to the plasma membrane (Fig. 5). Moreover, when WT was co-expressed with mutant proteins, the majority of WT co-localized with the mutants and remained in the intracellular compartment, indicating that the mutants may interfere with the normal trafficking of WT proteins (Fig. 6a). Using FRET analysis, we showed that this occurs because of direct protein–protein interaction between mutant and WT subunits (Fig. 6b). Therefore, the mutants may exert their dominant-negative effect by trapping WT intracellularly and preventing it from translocating to the plasma membrane. A recent report demonstrated that several KCNQ1 mutations cause trafficking errors and the mutant proteins are unable to translocate to the plasma membrane, and some mutations act in a dominant-negative fashion and have the ability to suppress the trafficking of the WT subunit [27,28].

4.3. Genotype-phenotype relationship

cRNAs were introduced in *Xenopus* oocytes in amounts mimicking the proportions of various transcripts of KCNQ1 observed in affected individuals. Ratios simulating those in affected individuals resulted in a pronounced reduction in the whole-cell potassium current, compared with ratios simulating those in normal individuals (Figs. 4c, d). This observation implies that a similar reduction might occur in the potassium current in cardiac myocytes of the mutant carriers, which may

contribute to the pathogenesis of LQTS. However, it should be noted that the quantitation of mRNA was performed in leukocytes, and it may not accurately reflect the mRNA ratio in the heart. Recently, we reported the identification of a Kcnq1 mutant rat, which carried an intragenic deletion in exon 7 of the Kcnq1 gene [29]. This mutant rat showed deafness due to the marked reduction of endolymph and prolonged QT interval in the ECG, further supporting our hypothesis that the deletion of exon 7 could lead to the phenotypes of LQTS. As far as we could determine, the proportions of mutant mRNAs were comparable in all the affected individuals, despite the fact that the QT_c interval and disease phenotype varied considerably (K-176 II-6: QTc 525 ms, history of syncope, WT: 53.5%, Δ7: 23.4%, Δ7–8: 17.7%, Δ8: 5.4%. K-176 III-2: QTc 404 ms, asymptomatic, WT: 56.6%, Δ7: 20.6%, Δ7–8: 17.7%, Δ8: 5.1%. K-176 III-3: QTc 448 ms, history of syncope, WT: 55.4%, Δ7: 26.5%, Δ7–8: 15.0%, Δ8: 15.0%). This suggests the presence of other modifying factors, which may be genetic or acquired, but the details are unknown.

4.4. Conclusions

We obtained data suggesting the mechanistic basis of the pathogenesis of LQTS caused by a common splicing mutation in KCNQ1. The functional abnormalities of mutant channels observed here may have critical impact on the cellular excitability, and thus contribute to the pathogenesis of LQTS.

Acknowledgments

We thank Dr. Naoyuki Kataoka (Institute for Viral Research, Kyoto University) for his helpful comments and critical reading of the manuscript.

This work was supported by a research grant from the Ministry of Education, Culture, Science, and Technology of Japan (M.H.) and a health sciences research grant (H18-Research on Human Genome-002) from the Ministry of Health, Labour and Welfare of Japan (M.H. and M.A.).

Appendix A. Supplementary data

Supplementary data associated with this article can be found, in the online version, at doi:10.1016/j.yjmcc.2006.12.015.

References

[1] Romano C. Congenital cardiac arrhythmia. Lancet 1965;17:658–9.
[2] Ward OC. A new familial cardiac syndrome in children. J Ir Med Assoc 1964;54:103–6.
[3] Moss AJ, Kass RS. Long QT syndrome: from channels to cardiac arrhythmias. J Clin Invest 2005;115:2018–24.
[4] Barhanin J, Lesage F, Guillemare E, Fink M, Lazdunski M, Romey G. K(V)LQT1 and lsK (minK) proteins associate to form the I(Ks) cardiac potassium current. Nature 1996;384:78–80.
[5] Sanguinetti MC, Curran ME, Zou A, Shen J, Spector PS, Atkinson DL, et al. Coassembly of K(V)LQT1 and minK (IsK) proteins to form cardiac I(Ks) potassium channel. Nature 1996;384:80–3.
[6] Wang Q, Curran ME, Splawski I, Burn TC, Millholland JM, Van Raay TJ, et al. Positional cloning of a novel potassium channel gene: KVLQT1 mutations cause cardiac arrhythmias. Nat Genet 1996;12:17–23.
[7] Murray A, Donger C, Fenske C, Spillman I, Richard P, Dong YB, et al. Splicing mutations in KCNQ1: a mutation hot spot at codon 344 that produces in frame transcripts. Circulation 1999;100:1077–84.
[8] Li H, Chen Q, Moss AJ, Robinson J, Goytia V, Perry JC, et al. New mutations in the KVLQT1 potassium channel that cause long-QT syndrome. Circulation 1998;97:1264–9.
[9] Kanters JK, Larsen LA, Orholm M, Agner E, Andersen PS, Vuust J, et al. Novel donor splice site mutation in the KVLQT1 gene is associated with long QT syndrome. J Cardiovasc Electrophysiol 1998;9:620–4.
[10] Kramer A. The structure and function of proteins involved in mammalian pre-mRNA splicing. Annu Rev Biochem 1996;65:367–409.
[11] Dreyfuss G, Kim VN, Kataoka N. Messenger–RNA-binding proteins and the messages they carry. Nat Rev, Mol Cell Biol 2002;3:195–205.
[12] Faustino NA, Cooper TA. Pre-mRNA splicing and human disease. Genes Dev 2003;17:419–37.
[13] Jongbloed R, Marcelis C, Velter C, Doevendans P, Geraedts J, Smeets H. DHPLC analysis of potassium ion channel genes in congenital long QT syndrome. Hum Mutat 2002;20:382–91.
[14] Ishii TM, Silvia C, Hirschberg B, Bond CT, Adelman JP, Maylie J. A human intermediate conductance calcium-activated potassium channel. Proc Natl Acad Sci U S A 1997;94:11651–6.
[15] Zaccolo M. Use of chimeric fluorescent proteins and fluorescence resonance energy transfer to monitor cellular responses. Circ Res 2004;94:866–73.
[16] Gu Y, Di WL, Kelsell DP, Zicha D. Quantitative fluorescence resonance energy transfer (FRET) measurement with acceptor photobleaching and spectral unmixing. J Microsc 2004;215:162–73.
[17] Hastings ML, Krainer AR. Pre-mRNA splicing in the new millennium. Curr Opin Cell Biol 2001;13:302–9.
[18] Weil D, D'Alessio M, Ramirez F, Eyre DR. Structural and functional characterization of a splicing mutation in the pro-alpha 2(I) collagen gene of an Ehlers–Danlos type VII patient. J Biol Chem 1990;265:16007–11.
[19] Akli S, Chelly J, Mezard C, Gandy S, Kahn A, Poenaru L. A "G" to "A" mutation at position −1 of a 5′ splice site in a late infantile form of Tay-Sachs disease. J Biol Chem 1990;265:7324–30.
[20] Grandchamp B, Picat C, de Rooij F, Beaumont C, Wilson P, Deybach JC, et al. A point mutation G—A in exon 12 of the porphobilinogen deaminase gene results in exon skipping and is responsible for acute intermittent porphyria. Nucleic Acids Res 1989;17:6637–49.
[21] Vidaud M, Gattoni R, Stevenin J, Vidaud D, Amselem S, Chibani J, et al. A 5′ splice-region G—C mutation in exon 1 of the human beta-globin gene inhibits pre-mRNA splicing: a mechanism for beta+-thalassemia. Proc Natl Acad Sci U S A 1989;86:1041–5.
[22] Krawczak M, Reiss J, Cooper DN. The mutational spectrum of single base-pair substitutions in mRNA splice junctions of human genes: causes and consequences. Hum Genet 1992;90:41–54.
[23] Nakai K, Sakamoto H. Construction of a novel database containing aberrant splicing mutations of mammalian genes. Gene 1994;141:171–7.
[24] Wijk R, van Wesel AC, Thomas AA, Rijksen G, van Solinge WW. Ex vivo analysis of aberrant splicing induced by two donor site mutations in PKLR of a patient with severe pyruvate kinase deficiency. Br J Haematol 2004; 125:253–63.
[25] Fairbrother WG, Yeh RF, Sharp PA, Burge CB. Predictive identification of exonic splicing enhancers in human genes. Science 2002;297:1007–13.
[26] Wang Z, Rolish ME, Yeo G, Tung V, Mawson M, Burge CB. Systematic identification and analysis of exonic splicing silencers. Cell 2004;119: 831–45.
[27] Yamashita F, Horie M, Kubota T, Yoshida H, Yumoto Y, Kobori A, et al. Characterization and subcellular localization of KCNQ1 with a heterozygous mutation in the C terminus. J Mol Cell Cardiol 2001;33:197–207.
[28] Wilson AJ, Quinn KV, Graves FM, Bitner-Glindzicz M, Tinker A. Abnormal KCNQ1 trafficking influences disease pathogenesis in hereditary long QT syndromes (LQT1). Cardiovasc Res 2005;67:476–86.
[29] Gohma H, Kuramoto T, Kuwamura M, Okajima R, Tanimoto N, Yamasaki KI, et al. WTC deafness Kyoto (dfk): a rat model for extensive investigations of Kcnq1 functions. Physiol Genomics 2006;24:198–206.